Zhao et al. *Zool. Res.* 2024, 45(4): 857−874
https://doi.org/10.24272/j.issn.2095-8137.2024.085

ZR | Zoological Research

Article Open Access

NLRP3-mediated autophagy dysfunction links gut microbiota dysbiosis to tau pathology in chronic sleep deprivation

Na Zhao[1,#], Xiu Chen[1,#], Qiu-Gu Chen[1], Xue-Ting Liu[1], Fan Geng[1], Meng-Meng Zhu[1], Fu-Ling Yan[1], Zhi-Jun Zhang[1], Qing-Guo Ren[1,2,*]

[1] *Department of Neurology*, *School of Medicine*, *Southeast University*, *Nanjing*, *Jiangsu* 210009, *China*
[2] *Department of Neurology*, *Affiliated Zhongda Hospital*, *Southeast University*, *Nanjing*, *Jiangsu* 210009, *China*

ABSTRACT

Emerging evidence indicates that sleep deprivation (SD) can lead to Alzheimer's disease (AD)-related pathological changes and cognitive decline. However, the underlying mechanisms remain obscure. In the present study, we identified the existence of a microbiota-gut-brain axis in cognitive deficits resulting from chronic SD and revealed a potential pathway by which gut microbiota affects cognitive functioning in chronic SD. Our findings demonstrated that chronic SD in mice not only led to cognitive decline but also induced gut microbiota dysbiosis, elevated NLRP3 inflammasome expression, GSK-3β activation, autophagy dysfunction, and tau hyperphosphorylation in the hippocampus. Colonization with the "SD microbiota" replicated the pathological and behavioral abnormalities observed in chronic sleep-deprived mice. Remarkably, both the deletion of NLRP3 in *NLRP3*$^{-/-}$ mice and specific knockdown of NLRP3 in the hippocampus restored autophagic flux, suppressed tau hyperphosphorylation, and ameliorated cognitive deficits induced by chronic SD, while GSK-3β activity was not regulated by the NLRP3 inflammasome in chronic SD. Notably, deletion of NLRP3 reversed NLRP3 inflammasome activation, autophagy deficits, and tau hyperphosphorylation induced by GSK-3β activation in primary hippocampal neurons, suggesting that GSK-3β, as a regulator of NLRP3-mediated autophagy dysfunction, plays a significant role in promoting tau hyperphosphorylation. Thus, gut microbiota dysbiosis was identified as a contributor to chronic SD-induced tau pathology via NLRP3-mediated autophagy dysfunction, ultimately leading to cognitive deficits. Overall, these findings highlight GSK-3β as a regulator of NLRP3-mediated autophagy dysfunction, playing a critical role in promoting tau hyperphosphorylation.

Keywords: Chronic sleep deprivation; Tau pathology; NLRP3 inflammasome; Autophagy; GSK-3β; Microbiota-gut-brain axis

INTRODUCTION

Adequate sleep is essential for optimal cognitive functioning, including decision-making, attention, learning, and memory (Donlea, 2019; Krueger et al., 2016). Both experimental and clinical studies have shown that sleep deprivation (SD) can increase the risk and progression of Alzheimer's disease (AD) (Lucey et al., 2021; Shi et al., 2018). Epidemiological data have also indicated that sleeping less than 5 h per night is associated with a two-fold increase in the incidence of dementia compared to sleeping for 7–8 h (Robbins et al., 2021). Experimental SD has been shown to impair learning and memory in both humans and mice (Lo et al., 2016; Wadhwa et al., 2019; Yin et al., 2017). Intracellular accumulation of hyperphosphorylated tau forming neurofibrillary tangles (NFTs) is a pathological hallmark of AD (Scheltens et al., 2021). Several studies have demonstrated that the sleep-wake cycle regulates tau levels in the cerebrospinal fluid (CSF) of humans and brain interstitial fluid (ISF) of mice, with SD increasing tau levels in both fluids and promoting the spread of tau pathology in the brain (Barthélemy et al., 2020; Holth et al., 2019). Despite strong evidence suggesting that SD can lead to AD-related pathological changes and impair cognitive functioning, the underlying mechanisms remain largely unknown.

The gut microbiota plays a crucial role in mediating the bidirectional interactions between the brain and gut, known as the microbiota-gut-brain axis (Mayer et al., 2022). This axis is closely related to human health, influencing neural development, neurotransmission, and behavior, with disruptions in the gut microbial community and composition linked to various neurological disorders, including both AD patients and mouse models (Morais et al., 2021; Vuotto et al., 2020; Zhang et al., 2017; Zhuang et al., 2018). Colonization with fecal microbiota from healthy wild-type (WT) mice has

Received: 18 March 2024; Accepted: 27 May 2024; Online: 28 May 2024
Foundation items: This study was supported by the National Natural Science Foundation of China (81870850) and Postgraduate Research & Practice Innovation Program of Jiangsu Province (KYCX23_0322)
[#]Authors contributed equally to this work
*Corresponding author, E-mail: renqingguo1976@163.com

been shown to improve tau-associated pathology, beta-amyloid plaque deposition, and cognitive decline in transgenic AD mice (Kim et al., 2020). Likewise, changes in gut microbial communities have been observed in animal models and humans with sleep disorders. Various sleep disruption protocols, including acute sleep restriction (Benedict et al., 2016; El Aidy et al., 2020), acute sleep-wake cycle shifts (Liu et al., 2020), chronic sleep fragmentation (Poroyko et al., 2016), and repeated sleep disruption (Bowers et al., 2020), have been shown to alter gut microbiota composition. However, further research is needed to determine whether the gut microbiota plays a critical role in cognitive deficits resulting from chronic SD and to elucidate the mechanisms of the microbiota-gut-brain axis in this process.

Interactions between the gut microbiota and brain primarily involve three parallel or interconnecting routes, including the endocrine system, immune system, and nerve pathways, all of which involve microbial products and metabolites (Cryan et al., 2019). In particular, microbial-immune interactions are key factors in the microbiota-gut-brain axis (Agirman et al., 2021; Pellegrini et al., 2020). Various studies have indicated that the gut microbiota can shape peripheral inflammatory responses, which may lead to neuroinflammation and neurodegeneration (Pearson-Leary et al., 2020; Pellegrini et al., 2018). Both our and previous studies have demonstrated that SD can disrupt the gut microbiota, contributing to both peripheral and central inflammatory responses and ultimately causing cognitive deficits, supporting the existence of a microbiota-gut-inflammation-brain axis (Wang et al., 2021; Zhao et al., 2023). NOD-like receptor family pyrin domain containing 3 (NLRP3) inflammasome-mediated neuroinflammation is considered a contributor to the pathogenesis and progression of AD (Feng et al., 2020). Therefore, it is plausible that the NLRP3 inflammasome serves as a crucial intersection in the microbiota-gut-brain axis related to cognitive deficits resulting from chronic SD.

Pathological aggregation of tau, a microtubule-associated protein that stabilizes neuronal microtubules and promotes axonal outgrowth, plays a major role in AD and other neurodegenerative disorders (Avila et al., 2004). Several factors contribute to tau aggregation, including imbalances between tau kinase and phosphatase activities, neuroinflammation, oxidative stress, and impaired tau clearance (Spillantini & Goedert, 2013). The autophagy-lysosome system, responsible for tau clearance, is essential for preventing the excessive accumulation of aggregated tau. Autophagy (macroautophagy) is a key conserved intracellular clearance process that delivers cytoplasmic contents to lysosomes for degradation (Levine & Kroemer, 2019). This process is vital for maintaining protein homeostasis by eliminating misfolded proteins, impaired organelles, and aggregated proteins (Kaushik & Cuervo, 2015). Compromised autophagy can lead to AD pathogenesis, especially tau pathology (Hamano et al., 2021; Zhang et al., 2021), with *in vitro* studies showing that inhibiting autophagic flux hampers tau clearance and subsequently induces aggregation of insoluble tau proteins (Hamano et al., 2008). Additionally, activation of the autophagy-lysosome pathway in tauopathy mouse models has a robust impact on attenuating tau pathology (Lachance et al., 2019; Polito et al., 2014). It is becoming increasingly clear that autophagy and the NLRP3 inflammasome are interconnected through reciprocal regulation (Biasizzo & Kopitar-Jerala, 2020; Tang et al., 2021). Many studies have shown that autophagy dysfunction can result in excessive NLRP3 inflammasome activation (Wang et al., 2017). Conversely, the NLRP3 inflammasome has also been shown to negatively regulate autophagy (Cosin-Roger et al., 2017; Wu et al., 2021). However, the interaction between autophagy and the NLRP3 inflammasome is complex and controversial, and their roles in the gut-brain crosstalk involved in cognitive deficits due to chronic SD remain underexplored and require further clarification.

Based on these observations, we hypothesize that the microbiota-gut-brain axis is involved in cognitive deficits resulting from chronic SD. Thus, we explored how the gut microbiota influences AD-related pathology and cognitive functioning in chronic SD. Our findings provide persuasive evidence that gut microbiota dysbiosis, driven by chronic SD, contributes to tau pathology via NLRP3-mediated autophagy dysfunction, ultimately leading to cognitive deficits. Additionally, we determined that GSK-3β, beyond acting as a tau kinase, serves as a regulator of NLRP3-mediated autophagy dysfunction, significantly promoting tau hyperphosphorylation and aggregation. This study enhances our understanding of the microbiota-gut-brain axis in cognitive deficits resulting from chronic SD and provides new perspectives for developing microbiome-based treatments for cognitive impairment caused by SD as well as insights into the interaction between AD and sleep disorders.

MATERIALS AND METHODS

Experimental design

This study was divided into four phases. Details on the experimental design are shown in Supplementary Figure S1.

Animals

Male C57BL/6J mice (6–8 weeks) were obtained from the Nanjing University Model Animal Research Center (Nanjing, China), while male *NLRP3*$^{-/-}$ mice (6–8 weeks) with a C57BL/6 background were obtained from the Jackson Laboratory. The animals were housed at the Southeast University Laboratory Animal Center (China) under specific pathogen-free conditions at a temperature of 22±2℃, humidity of 50%±5%, and standard 12:12 h light-dark cycle (lights on from 0700h to 1900h). All animal groups in the same batch were housed under identical conditions, including the same type of cage, bedding materials, and nestlets, all located in the same vivarium room. The mice were provided with the same autoclaved drinking water and food (Teklab certified global 18% protein rodent diet; cat. number T2018SC.15) *ad libitum*. Each mouse consumed approximately 4.0 mL of water per day, with no significant difference in water or food consumption among groups. The study employed a sterilized diet, sterilized cages, bedding, and water bottles, all autoclaved as a unit prior to cage changes, and cages were only opened within a HEPA-filtered animal transfer station when changing cages or collecting samples. All animal experiments were conducted in compliance with animal ethics and authorized by the Southeast University Institutional Animal Care and Use Committee (approval No. 20200418020). All efforts were made to minimize animal suffering and reduce the number of animals used.

Chronic SD procedures

Before conducting chronic SD (Bowers et al., 2020), all mice were raised for 1 week in chronic SD cages to acclimate to the

devices. The chronic SD cage consisted of an autoclaved, ventilated, transparent, microisolator chamber (height of 14 cm, diameter of 32 cm) with sterile bedding and standard laboratory food/water. A 30 cm long metal rod was fixed in the center at the bottom of the chamber. Throughout the chronic SD period, the metal rod was set up to spin at a steady speed (five revolutions per min) to keep the mice awake for 20 h each day (Zeitgeber time (ZT) 6–ZT2) for 21 consecutive days. Experimenters visually inspected mice at regular intervals during the SD windows to ensure that the metal rods were functioning properly and that the SD mice were awake. From ZT2 to ZT6, the metal rod remained stationary, allowing mice subjected to chronic SD to rest. ZT was defined as the number of hours after the onset of the light period (ZT0). Control mice allowed to sleep regularly were raised in identical SD devices in which the metal rod remained stationary during the chronic SD period.

Antibiotic treatment protocol

According to previously published protocols (Zhang et al., 2019), drinking water mixed with several antibiotics, including ciprofloxacin (Macklin, China, 200 mg/L), ampicillin (Meryer, China, 1 g/L), vancomycin (Macklin, China, 500 mg/L), metronidazole (Aladdin, China, 1 g/L), and imipenem plus cilastatin (MSD, USA, 250 mg/L), was administered to C57BL/6J mice for substantial depletion of the gut microbiota. The antibiotic solution was changed every 2–3 days, and the water bottles containing antibiotic solution were turned over every day. Antibiotic treatment was continued for 7 weeks. Finally, the antibiotic solution was replaced with sterile tap water 3 days before fecal microbiota transplantation.

Fecal sample collection

Before collecting fecal samples, mice were moved to autoclaved, ventilated, microisolator cages and provided with standard laboratory food and water (one mouse/cage). The mice were maintained in the cages under careful observation until 3–4 fresh fecal pellets (each mouse) were excreted. The mice were then removed from the cages and fresh fecal pellets from each animal were collected directly in sterile 1.5 mL centrifuge tubes using sterile cotton swabs. The fresh fecal samples were immediately stored at –80°C until fecal microbiota transplantation or microbiome analysis. All fecal samples were obtained between ZT8 and ZT12 to minimize circadian rhythm effects.

Fecal microbiota transplantation (FMT)

The FMT procedures followed previous published protocols (Liao et al., 2019), with some modifications. In brief, 200 μL of fecal dilution was transferred to recipient antibiotic-treated mice for 7 days via oral gavage. To prepare the dilution, fresh fecal samples were collected from chronic SD mice (SD group) and normal sleep mice (CON group). The fecal pellets from two groups were pooled and homogenized in anaerobic phosphate-buffered saline (PBS), respectively (25 mg stool/100 μL PBS). The samples were then vortexed for 5 min, followed by gentle centrifugation at 50 ×*g* for 3 min to precipitate the larger fecal particles. The supernatants of the two groups were then collected and diluted with sterile PBS (1:1). Finally, the antibiotic-treated mice were randomly divided into two groups and treated with 200 μL of fecal suspension from the CON and chronic SD groups, respectively, by oral gavage for 1 week. To determine whether differences in microbiota community structure between chronic SD and CON mice were maintained in the recipient mice, stools were harvested from recipient mice colonized with fecal microbiota from normal sleep mice (FMT-CON group) and chronic SD mice (FMT-SD group) 1 week post-FMT. Subsequently, 16S rRNA gene sequencing was performed on fecal samples from the CON, SD, FMT-CON, and FMT-SD groups. Principal coordinate analysis (PCoA) showed an obvious separation in the gut microbiota composition between the normal sleep donor mice and chronic SD donor mice. Likewise, the normal sleep microbiota recipient mice and chronic SD microbiota recipient mice exhibited a clear difference in gut microbial communities. In contrast, similarities were observed between the corresponding recipient and donor mice (Supplementary Figure S2). These results validated the fidelity of FMT.

Behavioral tests

The Morris water maze (MWM) and novel object recognition (NOR) tests were used to evaluate cognitive functioning in mice.

MWM test: The MWM test was applied to assess spatial learning and memory abilities of the research animals. The water maze consisted of a cylindrical water tank (diameter of 120 cm and height of 40 cm) with four quadrants. During the MWM test, the water tank was filled with water (depth of 30 cm and temperature of 21±1°C). During the acquisition trials, a platform (diameter of 10 cm) hidden 1.0 cm below the water surface was placed in the set quadrant and mice were trained to find the hidden platform with 60 s for 5 consecutive days. Each day, mice facing the tank wall were gently placed in the water from pseudo-random quadrants. If the mice did not locate the platform within 60 s, they were manually guided to the platform and required to remain on the platform for 30 s. The escape latencies of the mice were recorded. On day 6, the spatial probe trial was performed to determine memory retention. The mice were allowed to swim freely in the water tank for 60 s with the platform removed. Time spent in the target quadrant, number of platform crossings, and swimming paths were recorded using a video capture system.

NOR test: The NOR test was conducted to assess the tendency of mice to distinguish between a novel and familiar object, consisting of habituation, training, and testing stages. The mice were first individually conditioned to an open-field box for 10 min. One day later, two identical objects were placed into the two opposing corners of the open-field box. The mice were then allowed to explore the area and objects for 5 min. Time spent exploring the identical objects was recorded to determine any object preferences. During the testing phase, mice were placed in the same area with one familiar object and one novel object, then allowed to freely explore the objects for 5 min. Time spent exploring the familiar object (TF) and novel object (TN) was recorded. Exploration was recognized as orbiting, sniffing, and pawing the object. Recordings were ceased when the mice moved their heads 1 cm away from the object. After each trial, all objects and apparatus were cleaned using 70% ethanol to eliminate residual odor. A recognition index (RI) was calculated as RI=(TN/(TN+TF))×100%.

Tissue collection

One day after completing all behavior tests, the mice were sacrificed under deep anesthesia and brain tissues were promptly removed. Hippocampal samples were dissected from the brain tissues and stored at –80°C for subsequent

detection. Brain tissues were also fixed, dehydrated, embedded, and sectioned for immunofluorescence and immunohistochemical staining.

16S rRNA gene sequencing analysis

Cetyltrimethylammonium bromide (CTAB)/sodium dodecyl sulfate (SDS) was used to extract whole genome DNA from the fecal samples of both the chronic SD and control mice. The V3–V4 variable regions of the 16S rRNA gene were amplified and sequenced using the Illumina MiSeq/HiSeq2500 platform. The UPARSE package was employed to perform sequence analysis using the UPARSE-OTUref and UPARSE-OTU algorithms. We selected a representative sequence for each operational taxonomic unit (OTU) and annotated taxonomic information for each representative sequence using the RDP classifier. Sequences with a similarity of more than 97% were categorized as the same OTU. To investigate alpha-diversity (within samples) and beta-diversity (across samples), internal Perl scripts were utilized. Krona plots were used to display the relative abundance of bacterial diversity from phylum to species. Principal component analysis (PCA) was performed using QIIME before cluster analysis to minimize the dimension of original variables. PCoA facilitated the extraction and visualization of principal coordinates from multidimensional, complicated data. Both unweighted and weighted-UniFrac distance, known as the phylogenetic measures of beta-diversity, were calculated using QIIME to explore differences in community composition between different groups. STAMP was used to verify dissimilarities in the abundance of individual taxonomies between the chronic SD and control groups.

Immunohistochemical and immunofluorescence staining

Brain tissues were fixed in 4% paraformaldehyde for 24 h, then transferred to ascending grades of ethyl alcohol for dehydration, followed by immersion in xylene and embedding in paraffin. The paraffin-embedded blocks were cut into sections (5 μm thick) for immunohistochemical and immunofluorescence staining.

For immunofluorescence staining, the paraffin-embedded brain sections were baked at 60°C for 2 h, dewaxed in xylene three times, sequentially placed in a gradient ethanol, and rinsed with distilled water twice. The sections were then immersed in sodium citrate solution (pH=6.0) for antigen retrieval by microwave for 20 min. After cooling down to room temperature, the sections were washed with PBS three times and blocked with 3% bovine serum albumin (BSA) at room temperature for 30 min, followed by incubation with monoclonal antibodies, including anti-phospho-tau (Ser396) (1:1 000, Abcam, UK) and anti-NLRP3 (1:200, AdipoGen, USA) at 4°C overnight in a wet box. The following day, the sections were washed with PBS three times (5 min each) and incubated with appropriate secondary antibodies (1:1 000, Abcam, UK) for 1 h in a wet box. After washing with PBS for 3×5 min, nuclei were counterstained with 4',6-diamidino-2-phenylindole (DAPI) mounting medium at room temperature for 20 min. The stained sections were observed and imaged using a confocal microscope (Zeiss, Germany).

For immunohistochemical staining, the paraffin-embedded brain sections were deparaffinized, rehydrated, and heated in a microwave oven for 20 min in Tris-EDTA (pH 9.0) for antigen retrieval. Endogenous peroxidase activity was blocked with 0.3% H_2O_2 in absolute methanol for 30 min and nonspecific sites were blocked with 3% BSA for 30 min at room temperature. The sections were then incubated with primary antibodies at optimized dilutions at 4°C overnight. The next day, the sections were washed twice with PBS and subsequently incubated with biotin-labeled secondary antibodies for 1 h at 37°C. The immunoreaction was developed using a Histostain TM-SP kit (ThermoFisher Scientific, USA). An enzyme substrate 3,3'-diaminobenzidine (DAB) Substrate-Kit (Vector) was used to visualize the signal, with the sections then counterstained with hematoxylin. The sections were imaged using a microscope (Olympus BX60, Japan).

Western blotting

Hippocampal tissues were collected and lysed on ice for 30 min with RIPA lysis buffer consisting of 50 mmol/L Tris-HCl (pH 7.0), 1 mmol/L EDTA, 0.1 mmol/L phenylmethylsulfonyl fluoride (PMSF), 1 mmol/L benzamidine, 0.5 mmol/L isobutylmethylxanthine, and multiple inhibitors. The samples were then homogenized, with the homogenates then centrifuged at 12 000 r/min for 15 min at 4°C. The resulting supernatants were collected, and the protein concentrations of the supernatants were determined using a bicinchoninic acid (BCA) protein assay kit (Beyotime, China). Protein samples diluted with loading buffer (6×concentrate; Beyotime, China) were boiled for 8 min, then stored at –20°C.

To separate proteins, equal amounts of protein samples were subjected to 7.5%–12.5% sodium dodecyl sulfate-polyacrylamide gel electrophoresis (SDS-PAGE), then transferred to polyvinylidene difluoride (PVDF) membranes (Immobilon Transfer Membrane, Millipore, USA) at 300 mA for 0.5–2 h and blocked with 5% (w/v) nonfat milk for 2 h at room temperature. The membranes were incubated with primary antibodies in 5% (w/v) BSA at 4°C overnight, then washed with TBST for 8 min three times and incubated with appropriate goat anti-rabbit or goat anti-mouse peroxidase-conjugated secondary antibodies (1:5 000, Pierce, USA) for 1 h at room temperature. The blots were visualized using an enhanced chemiluminescence substrate (ECL, Millipore, USA) and integral optical density values (IOD) were measured by Image Pro-Plus v.6.0 software. The β-actin protein level was used as the internal control. Primary antibodies used included: anti-phospho-tau (Thr231) (1:1 000, Abcam, UK), anti-phospho-tau (Ser396) (1:5 000, Abcam, UK), anti-tau-1 (1:1 000, Merck Millipore, USA), anti-tau-5 (1:1 000, Abcam, UK), anti-total-GSK-3β (GSK-3β) (1:1 000, Cell Signaling Technology, USA), anti-phospho-GSK-3β (Ser9) (1:1 000, Cell Signaling Technology, USA), anti-NLRP3 (1:2 000, AdipoGen, USA), anti-IL-1β (1:1 000, Abcam, UK), anti-IBA-1 (1:1 000, Wako, Japan), anti-Beclin-1 (1:1 000, Cell Signaling Technology, USA), anti-LC3B (1:1 000, Cell Signaling Technology, USA), anti-SQSTM1/p62 (1:1 000, Merck Millipore, USA), and anti-β-actin (1:1 000, Abcam, UK).

Reverse transcription-quantitative real-time polymerase chain reaction (RT-qPCR)

Total RNA was isolated from hippocampal tissues using TRIzol reagent (ThermoFisher Scientific, USA). The purity, quantity, and integrity of RNA were measured using a Nano-Drop 8000 Spectrophotometer (ThermoFisher Scientific, USA). The Omniscript Reverse Transcription Kit (Qiagen, Japan) was applied in accordance with the manufacturer's instructions to generate cDNA from a total of 1 μg of RNA. Fast SYBR GreenER Master Mix (ThermoFisher Scientific, USA) was utilized according to the manufacturer's

recommendations for qPCR assembly using a Real-Time PCR System (Applied Biosystems 7300). The $2^{-\Delta\Delta CT}$ method, which calculates the relative quantification of a target gene normalized to the GAPDH gene, was used to determine mRNA expression. The PCR primers used included: mouse total tau: forward 5'-GAA CCA CCA AAA TCC GGA GA-3'; reverse 5'-CTC TTA CTA GCT GAT GGT GAC-3'; GAPDH: forward 5'-ACA ACT TTG GTA TCG TGG AAG G-3'; reverse 5'-GCC ATC ACG CCA CAG TTT C-3'.

Knockdown of NLRP3 using adeno-associated virus (AAV) delivery

AAV vectors containing a non-specific sequence (CGC TGA GTA CTT CGA AAT GTC) or short hairpin RNA targeting NLRP3 (CCA GGA TCC TCT TCC TCA TA) were designed and obtained from GeneChem (China). Mice received a microinjection of AAV vectors carrying green fluorescent protein (GFP) (AAV-GFP) or targeting NLRP3 (AAV-NLRP3) into the hippocampus. In brief, mice were anesthetized with 4% chloral hydrate (intraperitoneal injection), then immobilized in a stereotaxic apparatus (David Kopf Instruments, USA). Two small holes (diameter of 1 mm) were then drilled in precise sites of the bared skull (AP: −2.0 mm, ML: ±2.0 mm, DV: −2.0 mm), followed by microinjection of 2.0 μL of AAV vectors (AAV-GFP: 11.4×10^{12} vg/mL or AAV-NLRP3: 8.33×10^{12} vg/mL) into the bilateral hippocampus with a microsyringe (1.0 μL per side, 0.2 μL/min), which was kept in place for 10 min following injection to avoid viral particle backflow. Vectors encoded with enhanced GFP help verify successful infusion via fluorescence microscopy. Western blotting was also carried out to confirm the effects of transfection.

Cell culture

Primary hippocampal neurons were obtained from embryonic day 18 (E18) WT mice and *NLRP3*$^{-/-}$ mice. The neurons were grown in 6-well or 12-well plates covered with Poly-D-Lysine/Laminin (Sigma-Aldrich, USA) for 3 h to allow neurons to attach to the plates. Neurobasal medium with 25 mmol/L glutamate, 2% B27, and 0.5 mmol/L glutamine (ThermoFisher Scientific, USA) was applied to the culture neurons. Every 3 days, half of the culture medium was replaced with fresh neurobasal medium. All neurons were kept in CO_2 incubators (temperature 37℃, CO_2 5%, humidity 95%). After 7 days of culture, the primary hippocampal neurons were treated with Akt inhibitor MK-2206 (Selleckchem, USA). Finally, primary neurons subjected to western blotting and immunofluorescence staining. Each condition was conducted in three biological replicates.

Statistical analysis

All collected data were shown as mean±standard error of the mean (SEM) and statistical analyses were conducted using GraphPad Prism v.9.0 (GraphPad Software, USA). Differences between two individual groups were compared using unpaired Student's *t*-test. The Mann-Whitney *U* test was employed for non-normally distributed data, while Welch's *t*-test was used for data with unequal variances. One-way analysis of variance (ANOVA), coupled with Tukey's *post hoc* test for multiple comparisons was used to determine statistical differences among three or more groups. Data from different groups at different time points, such as escape latencies during 5 day MWM spatial training, were compared using repeated measures two-way ANOVA. Differences were regarded as statistically significant at $P<0.05$. Each experiment was carried out with at least three replicates.

RESULTS

Chronic SD induced cognitive deficits and altered gut microbiota composition in mice

The MWM test is typically applied to assess cognitive functioning. In the training trials, the mice subjected to chronic SD exhibited longer escape latencies than the mice allowed to sleep regularly, especially on days 4 and 5 (group: $F_{(1,16)}=16.004$, $P=0.0013$, $\eta_p^2=0.533$; day: $F_{(4,56)}=152.721$, $P<0.0001$, $\eta_p^2=0.916$; interaction: $F_{(4,56)}=3.063$, $P=0.0237$, $\eta_p^2=0.180$; day 4: $P=0.0158$; day 5: $P=0.0029$, Figure 1A). In the spatial probe trial, the chronic SD mice exhibited poorer performance compared to control mice, as evidenced by the lower percentage of time spent in the target quadrant ($t_{14}=3.945$, $P=0.0015$, Cohen's d=1.988, Figure 1B) and fewer platform crossings ($t_{14}=3.024$, $P=0.0091$, Cohen's d=1.525, Figure 1C). The heatmaps of swimming paths indicated that, compared to mice in the chronic SD group, the control group mice swam more frequently in the platform and surrounding areas (Figure 1D). These findings suggest that chronic SD impairs spatial learning and memory ability in mice.

Our previous study revealed distinct differences in the gut microbial communities between the chronic SD and control groups (Zhao et al., 2023). Sequences were annotated into OTUs. As depicted in the Venn diagram, the two groups shared 1 101 OTUs, with 298 OTUs unique to the control group and 203 OTUs unique to the chronic SD group (Supplementary Figure S3A). PCoA based on the weighted-UniFrac index exhibited a clear difference in gut microbiota composition between the two groups (Supplementary Figure S3B). At the phylum level, Proteobacteria, Bacteroidetes, and Firmicutes were the dominant bacteria, comprising most of the gut microbiota community. Compared to the control group, the chronic SD group exhibited a marked increase in the relative abundance of Bacteroidetes from 56% to 71%, while the relative abundances of Proteobacteria and Firmicutes decreased (Supplementary Figure S3C). Additionally, at the genus level, the chronic SD group showed an increased relative abundance of *Odoribacter* and a concomitant reduction in *Lactobacillus* (Supplementary Figure S3D). Overall, these findings indicate that chronic SD alters the composition of gut microbiota in mice.

Chronic SD induced tau hyperphosphorylation and GSK-3β activation in the hippocampus of mice

Next, we investigated the influence of chronic SD on tau phosphorylation. Compared to control mice, the levels of tau phosphorylation at the Thr231 (pT231) and Ser396 (pS396) sites were significantly up-regulated in the hippocampus of chronic SD mice (pT231: $t_4=3.940$, $P=0.0170$; pS396: $t_4=4.896$, $P=0.0081$, Figure 2A), as verified by immunofluorescence staining (Figure 2C). In addition, the level of Tau-1 was decreased in the hippocampus of chronic SD mice (Tau-1: $t_4=4.890$, $P=0.0081$, Figure 2A). Lower expression of Tau-1, a non-phosphorylated tau located at the Ser198/199/202 sites, reflected an increase in tau phosphorylation. Interestingly, the level of total tau (Tau-5) in the chronic SD group was higher than that in the control group (Tau-5: $t_4=4.902$, $P=0.0080$, Figure 2A). However, no significant difference in the mRNA level of tau was observed

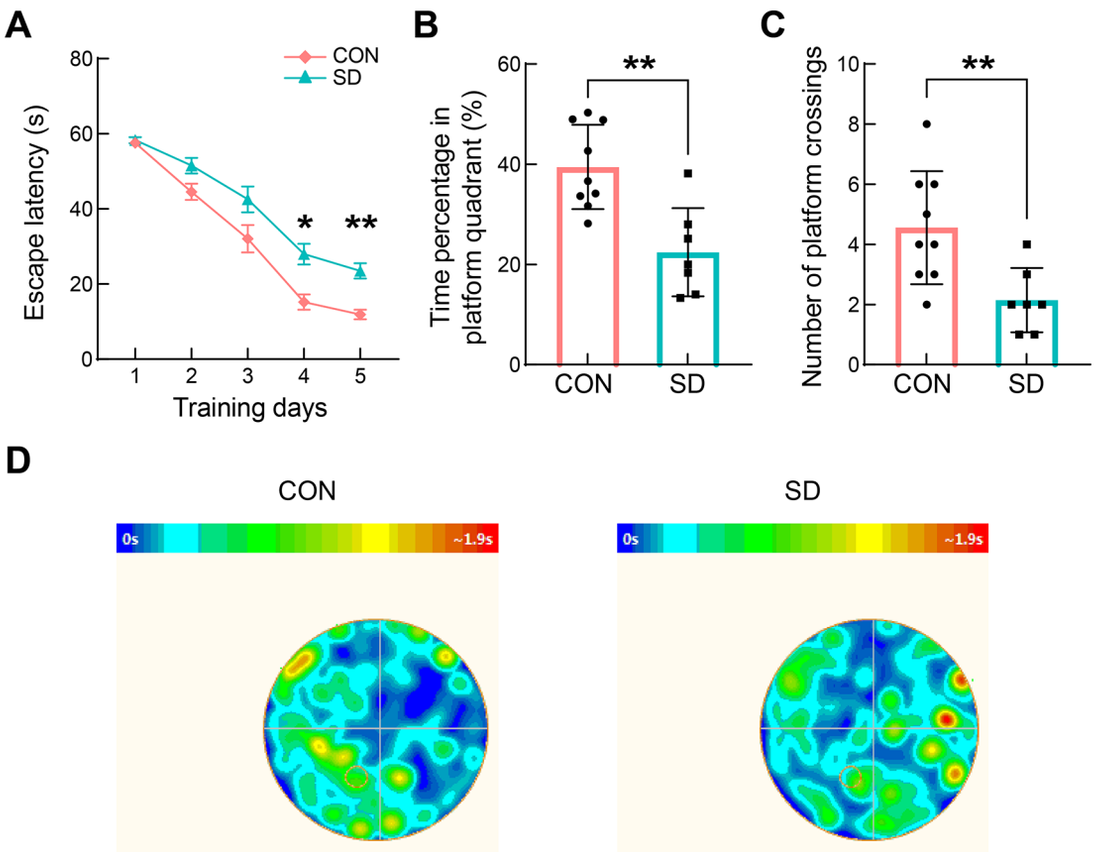

Figure 1 Chronic SD induced cognitive deficits in mice

A: Escape latency of chronic SD mice and controls for five consecutive training days in the MWM test. B: Percentage of time spent in platform quadrant in spatial probe trial of the MWM test. C: Number of platform crossings in spatial probe trial of the MWM test. D: Representative heatmaps of swimming paths in spatial probe trial of the MWM test. All data are expressed as mean±SEM. CON n=9 mice/group; SD n=7 mice/group. Data were considered significant at *: P<0.05, **: P<0.01, ***: P<0.001, ****: P<0.0001. ns: Not significant. Means were compared using two-way repeated measures ANOVA with Bonferroni *post hoc* comparison in panel A and Student's *t*-test in panel B, C. SD: Chronic sleep-deprived mice; CON: Normal sleep littermate controls,

between the two groups (t_6=0.285, P=0.7852, Figure 2B).

The activity of GSK-3β, known to act as an important tau kinase, was measured by western blotting. The chronic SD mice exhibited a down-regulation in phosphorylated GSK-3β at the Ser9 site compared to the control mice, resulting in the activation of GSK-3β (pS9-GSK-3β: t_4=7.390, P=0.0018, Figure 2D). In addition, no differences were found in the level of total GSK-3β (t-GSK-3β: t_4=0.8703, P=0.4332, Figure 2D). These findings suggest that chronic SD can induce intracellular tau hyperphosphorylation and excessive activation of GSK-3β in the hippocampus of mice.

Chronic SD activated NLRP3 inflammasome and inhibited autophagy in the hippocampus of mice

The levels of interleukin-1β (IL-1β) and NLRP3 in the hippocampus of mice were measured by western blot analysis. Results indicated that the expression levels of IL-1β and NLRP3 were significantly elevated in the hippocampus of the chronic SD group compared to the control group (NLRP3: t_4=5.292, P=0.0061; IL-1β: t_4=7.049, P=0.0021, Figure 3A). Up-regulation of NLRP3 expression in the hippocampus of the chronic SD group was also confirmed through immunofluorescence staining (Figure 3B). The expression level of IBA-1, indicative of microglial activation, was also elevated in the hippocampus of chronic SD mice (IBA-1: t_4=3.570, P=0.0234, Figure 3A). Based on detection of autophagy activity, the levels of several autophagosome markers, including Beclin-1, microtubule-associated protein light chain 3 (LC3)-II, and conversion of LC3-I to LC3-II, were decreased in the hippocampus of chronic SD mice compared to control mice (Beclin-1: t_4=4.277, P=0.0129; LC3-II: t_4=5.094, P=0.0070; LC3-II/I: t_4=4.643, P=0.0097, Figure 3C). In addition, the expression of SQSTM1/p62 was significantly increased in the chronic SD group (p62: t_4=5.002, P=0.0075, Figure 3C). These findings indicate that chronic SD induces NLRP3 inflammasome activation and blocks autophagic flux in the hippocampus of mice.

SD microbiota transplantation impaired cognitive function, increased tau phosphorylation, and activated GSK-3β in mice

FMT was performed to examine whether changes in gut microbiota from chronic SD mice contribute to pathological brain abnormalities and behavioral alterations. Gut microbiota from normal sleep mice or chronic SD mice were transplanted into healthy WT mice via oral gavage for 1 week. Notably, FMT from chronic SD mice, but not from normal sleep mice, resulted in a significant reduction in the RI of the NOR test, indicating cognitive decline in the chronic SD microbiota recipient mice (t_{15}=3.057, P=0.0080, Cohen's d=1.485, Figure 4A, B). Western blot analysis revealed increased levels of phosphorylated tau (pS396-tau and pT231-tau) and

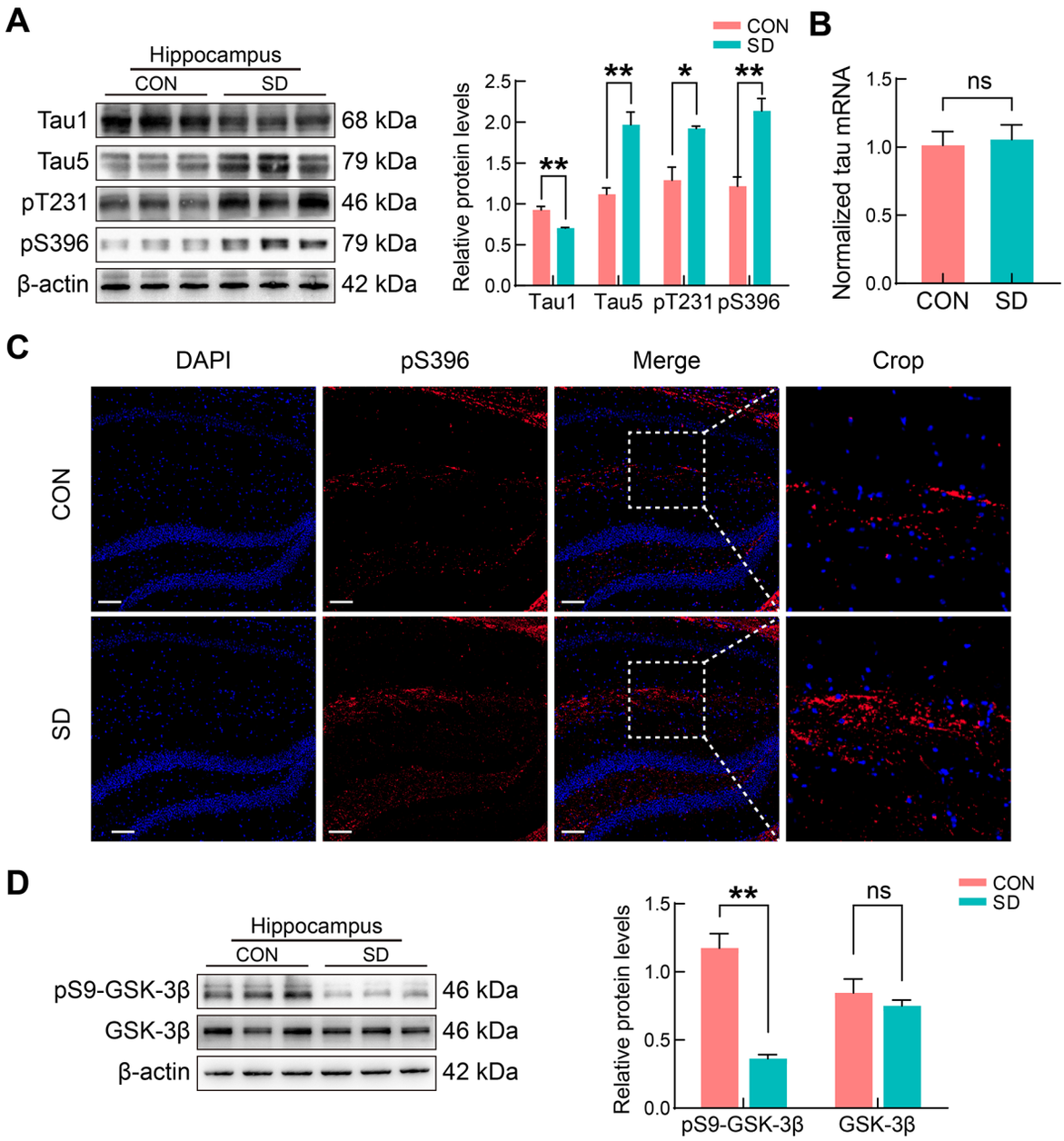

Figure 2 Chronic SD induced tau hyperphosphorylation and GSK-3β activation in the hippocampus of mice

A: Protein levels of Tau-1, Tau-5, pS396-tau, and pT231-tau were determined by western blotting in hippocampus of chronic SD mice and controls. B: mRNA level of tau measured by qPCR in hippocampus of chronic SD mice and controls. C: Representative immunofluorescence staining against pS396-tau in hippocampal regions (CA1, CA3, and DG). Magnification ×10, Scale bar: 100 μm. D: Protein levels of p-GSK-3β (Ser9) and total GSK-3β were determined by western blotting in hippocampus of chronic SD mice and controls. All data are expressed as mean±SEM. n=3 mice/group. β-actin was used as the loading control in western blot analysis. Data were considered significant at *: P<0.05, **: P<0.01, ***: P<0.001, ****: P<0.0001 by Student's t-test. ns: Not significant. SD: Chronic sleep-deprived mice; CON: Normal sleep littermate controls.

reduced levels of non-phosphorylated tau (Tau-1) in the hippocampus of chronic SD microbiota recipient mice compared to control recipient mice (pT231: t_4=3.079, P=0.0370; pS396: t_4=8.546, P=0.0010; Tau-1: t_4=5.932, P=0.0040, Figure 4C). Immunofluorescence staining against pS396-tau also demonstrated that colonization with chronic SD microbiota increased tau phosphorylation at the Ser396 site in the hippocampus of recipient mice (Figure 4D). Additionally, the expression of total tau (Tau-5) was enhanced in the hippocampus of chronic SD microbiota recipient mice (Tau-5: t_4=3.964, P=0.0166, Figure 4C). Further, an obvious decrease in the phosphorylation of GSK-3β at the Ser9 site, with no change in total GSK-3β levels, was observed in the hippocampus of recipient mice treated with chronic SD microbiota, suggesting pronounced activation of GSK-3β (pS9-GSK-3β: t_4=4.533, P=0.0106; t-GSK-3β: t_4=0.4500, P=0.6760, Figure 4E).

SD microbiota transplantation inhibited autophagic flux and enhanced NLRP3 inflammasome activity

As shown in western blot analysis, the transfer of gut microbiota derived from chronic SD mice resulted in the inhibition of autophagy, as indicated by the down-regulation of LC3-II, Beclin-1, and the LC3-II/LC3-I ratio, and up-regulation of SQSTM1/p62 in the hippocampus of chronic SD microbiota recipient mice (Beclin-1: t_4=4.370, P=0.0120; LC3-II: t_4=3.782,

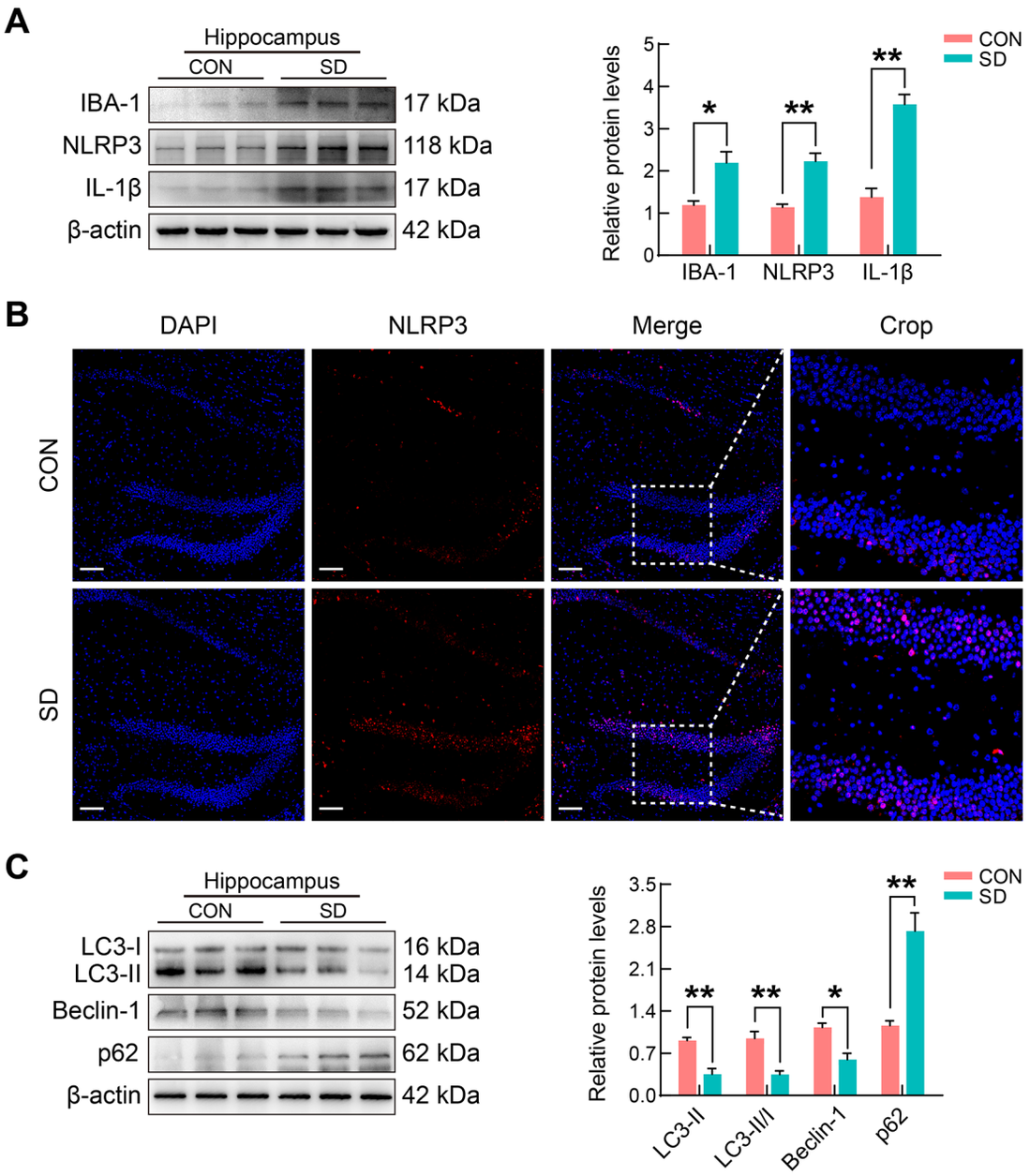

Figure 3 Chronic SD induced NLRP3 inflammasome activation and autophagy inhibition in the hippocampus of mice

A: Protein levels of IBA-1, NLRP3, and IL-1β were determined by western blotting in hippocampus of chronic SD mice and controls. B: Representative immunofluorescence staining against NLRP3 was performed on hippocampal regions (CA1, CA3, and DG). Magnification ×10, Scale bar: 100 μm. C: Protein levels of Beclin-1, LC3-II, SQSTM1/p62 and LC3-II/LC3-I ratio were determined by western blotting in hippocampus of chronic SD mice and controls. All data are expressed as mean±SEM. *n*=3 mice/group. β-actin was used as the loading control in western blot analysis. Data were considered significant at *: $P<0.05$, **: $P<0.01$, ***: $P<0.001$, ****: $P<0.0001$ by Student's *t*-test. ns: Not significant. SD: Chronic sleep-deprived mice; CON: Normal sleep littermate controls.

P=0.0194; LC3-II/I: t_4=4.054, P=0.0154; p62: t_4=4.464, P=0.0111, Figure 5A). Concomitantly, compared to the normal sleep microbiota recipient mice, the chronic SD microbiota recipient mice displayed higher expression levels of IL-1β, NLRP3, and IBA-1 in the hippocampus (IBA-1: t_4=4.465, P=0.0111; NLRP3: t_4=3.358, P=0.0284; IL-1β: t_4=4.298, P=0.0127, Figure 5B, C).

Pathological and behavioral changes from chronic SD were nearly reversed in *NLRP3*$^{-/-}$ mice

Next, we explored the role of the NLRP3 inflammasome in chronic SD. Different from WT mice, *NLRP3*$^{-/-}$ mice showed no NLRP3 expression and very low IL-1β and IBA-1 expression in the hippocampus, regardless of their exposure to chronic SD or normal sleep (IBA-1: $F_{(3,8)}$=26.273, P=0.0002; WT/CON vs. WT/SD: P=0.0011; *NLRP3*$^{-/-}$/CON vs. *NLRP3*$^{-/-}$/SD: P=0.9502; WT/CON vs. *NLRP3*$^{-/-}$/CON: P=0.4410; WT/SD vs. *NLRP3*$^{-/-}$/SD: P=0.0004, NLRP3: $F_{(3,8)}$=61.374, P<0.0001; WT/CON vs. WT/SD: P=0.0002; *NLRP3*$^{-/-}$/CON vs. *NLRP3*$^{-/-}$/SD: P=0.9995; WT/CON vs. *NLRP3*$^{-/-}$/CON: P=0.0255; WT/SD vs. *NLRP3*$^{-/-}$/SD: P=0.0001, IL-1β: $F_{(3,8)}$=20.457, P=0.0004; WT/CON vs. WT/SD: P=0.0036; *NLRP3*$^{-/-}$/CON vs. *NLRP3*$^{-/-}$/SD: P=0.9329; WT/CON vs. *NLRP3*$^{-/-}$/CON: P=0.3386; WT/SD vs. *NLRP3*$^{-/-}$/SD: P=0.0009, Figure 6F).

Cognitive performance was evaluated using the NOR test. After chronic SD, cognitive functioning was markedly disrupted

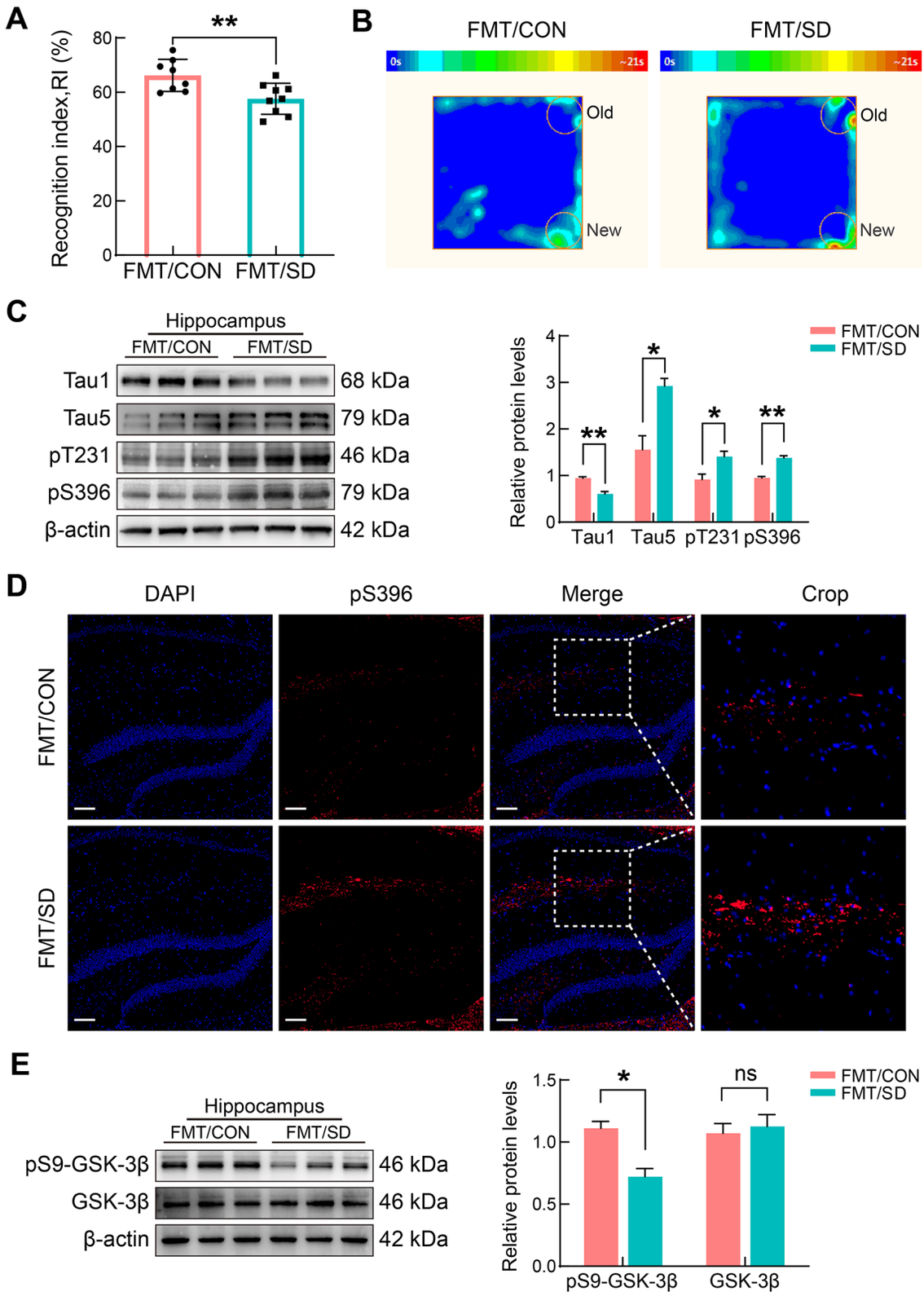

Figure 4 SD microbiota transplantation impaired cognitive function, increased tau phosphorylation, and activated GSK-3β

A, B: Recognition index (A) and map of trajectory (B) in the novel object recognition test. C: Protein levels of Tau-1, Tau-5, pS396-tau, and pT231-tau were determined by western blotting in hippocampus of chronic SD microbiota recipient mice and control microbiota recipient mice. D: Representative immunofluorescence staining against pS396-tau was performed on hippocampal regions (CA1, CA3, and DG). Magnification ×10, Scale bar: 100 μm. E: Protein levels of p-GSK-3β (Ser9) and total GSK-3β were determined by western blotting in hippocampus of chronic SD microbiota recipient mice and controls. All data are expressed as mean±SEM. A, B: FMT/CON n=8 mice/group; FMT/SD n=9 mice/group. C–E: n=3 mice/group. β-actin was used as the loading control in western blot analysis. Data were considered significant at *: P<0.05, **: P<0.01, ***: P<0.001, ****: P<0.0001 by Student's t-test. ns: Not significant. FMT-SD: Fecal microbiota transplantation (FMT) of chronic sleep-deprived mice; FMT-CON: Fecal microbiota transplantation (FMT) of control normal sleep mice.

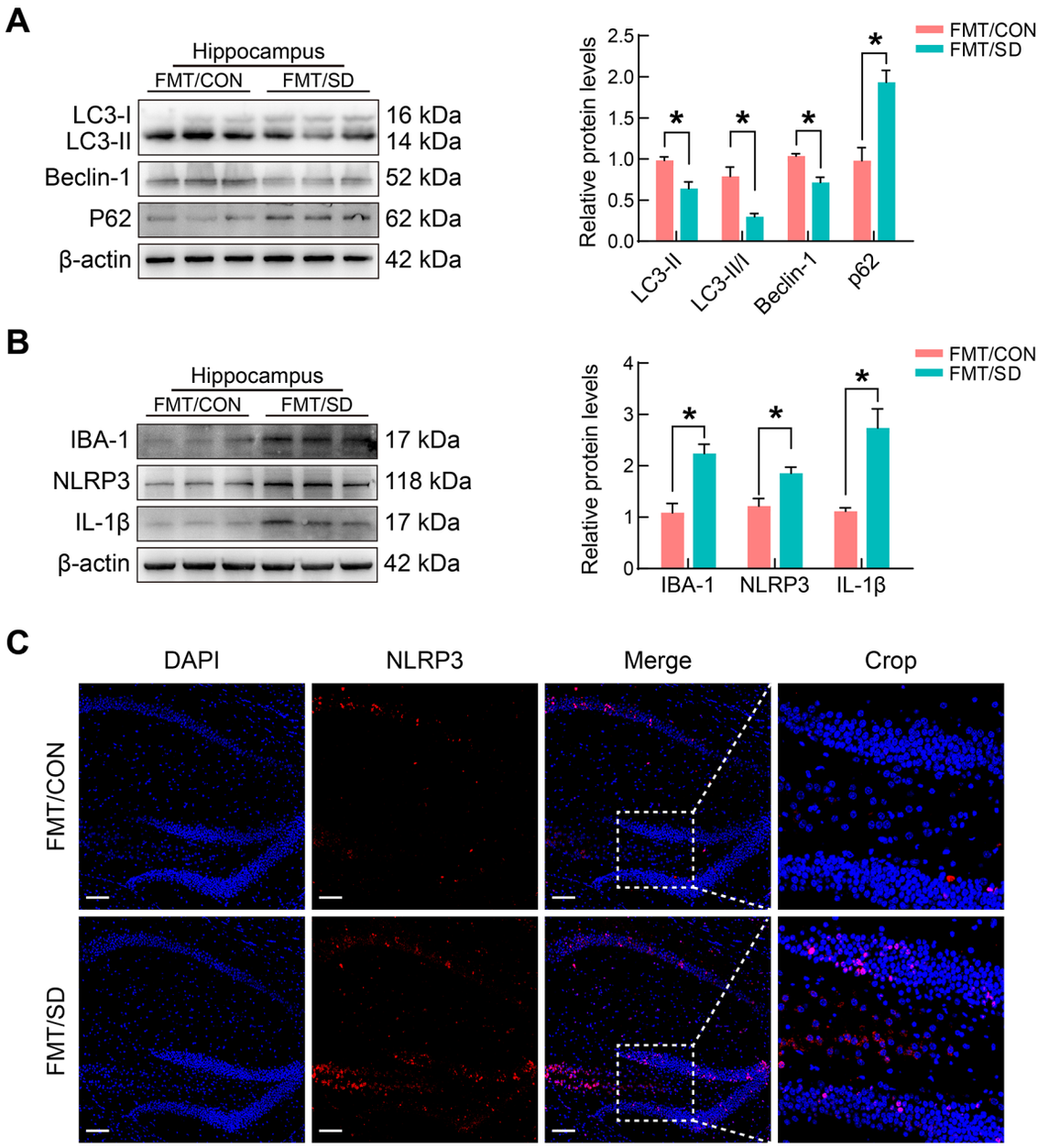

Figure 5 SD microbiota transplantation inhibited autophagic flux and enhanced NLRP3 inflammasome activity

A: Protein levels of Beclin-1, LC3-II, SQSTM1/p62, and the LC3-II/LC3-I ratio were determined by western blotting in hippocampus of chronic SD microbiota recipient mice and control microbiota recipient mice. B: Protein levels of IBA-1, NLRP3, and IL-1β were determined by western blotting in hippocampus of chronic SD microbiota recipient mice and controls. C: Representative immunofluorescence staining against NLRP3 was performed on hippocampal regions (CA1, CA3, and DG). Magnification ×10, Scale bar: 100 μm. All data are expressed as mean±SEM. n=3 mice/group. β-actin was used as the loading control in western blot analysis. Data were considered significant at *: P<0.05, **: P<0.01, ***: P<0.001, ****: P<0.0001 by Student's t-test. ns: Not significant. FMT-SD: Fecal microbiota transplantation (FMT) of chronic sleep-deprived mice; FMT-CON: Fecal microbiota transplantation (FMT) of control normal sleep mice.

in WT mice but not in *NLRP3*$^{-/-}$ mice. Chronic SD resulted in an obvious decline in the RI, which improved by NLRP3 inflammasome deficiency ($F_{(3,25)}$=15.191, P<0.0001; WT/CON vs. WT/SD: P=0.0001; *NLRP3*$^{-/-}$/CON vs. *NLRP3*$^{-/-}$/SD: P=0.0424; WT/CON vs. *NLRP3*$^{-/-}$/CON: P=0.5513; WT/SD vs. *NLRP3*$^{-/-}$/SD: P=0.0064, Figure 6A, B). Correspondingly, chronic SD decreased the level of Tau-1 and elevated the levels of pT231-tau, pS396-tau, and Tau-5 in the hippocampus of WT mice, which were not observed in the hippocampus of *NLRP3*$^{-/-}$ mice (Tau-1: $F_{(3,8)}$=31.399, P<0.0001; WT/CON vs. WT/SD: P=0.0002; *NLRP3*$^{-/-}$/CON vs. *NLRP3*$^{-/-}$/SD: P=0.7797; WT/CON vs. *NLRP3*$^{-/-}$/CON: P=0.9999; WT/SD vs. *NLRP3*$^{-/-}$/SD: P=0.0004, Tau-5: $F_{(3,8)}$=12.070, P=0.0024; WT/CON vs. WT/SD: P=0.0036; *NLRP3*$^{-/-}$/CON vs. *NLRP3*$^{-/-}$/SD: P=0.4571; WT/CON vs. *NLRP3*$^{-/-}$/CON: P=0.9768; WT/SD vs. *NLRP3*$^{-/-}$/SD: P=0.0453, pT231: $F_{(3,8)}$=12.048, P=0.0025; WT/CON vs. WT/SD: P=0.0056; *NLRP3*$^{-/-}$/CON vs. *NLRP3*$^{-/-}$/SD: P=0.8212; WT/CON vs. *NLRP3*$^{-/-}$/CON: P=0.9661; WT/SD vs. *NLRP3*$^{-/-}$/SD: P=0.0094, pS396: $F_{(3,8)}$=19.367, P=0.0005; WT/CON vs. WT/SD: P=0.0009; *NLRP3*$^{-/-}$/CON vs. *NLRP3*$^{-/-}$/SD: P=0.5685; WT/CON vs. *NLRP3*$^{-/-}$/CON: P=0.9988; WT/SD vs. *NLRP3*$^{-/-}$/SD: P=0.0034, Figure 6C, D). In contrast to WT mice, no significant differences in the expression levels of LC3-II,

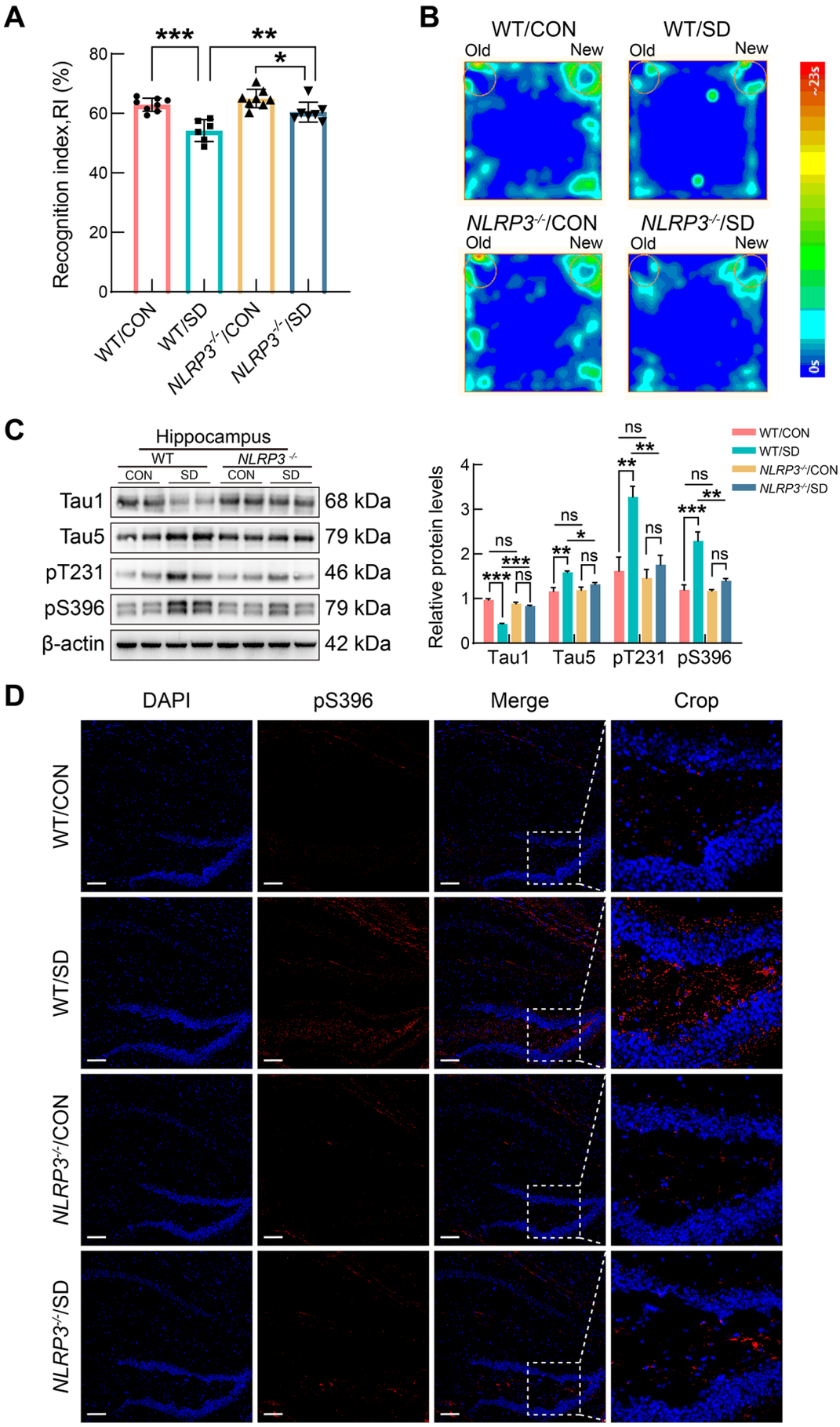
A
Recognition index,RI (%)
WT/CON
WT/SD
NLRP3-/-/CON
NLRP3-/-/SD
B
WT/CON
WT/SD
NLRP3-/-/CON
NLRP3-/-/SD
Old
New
~23s
0s
C
Hippocampus
WT
NLRP3 -/-
CON
SD
Tau1
Tau5
pT231
pS396
β-actin
68 kDa
79 kDa
46 kDa
79 kDa
42 kDa
Relative protein levels
D
DAPI
pS396
Merge
Crop

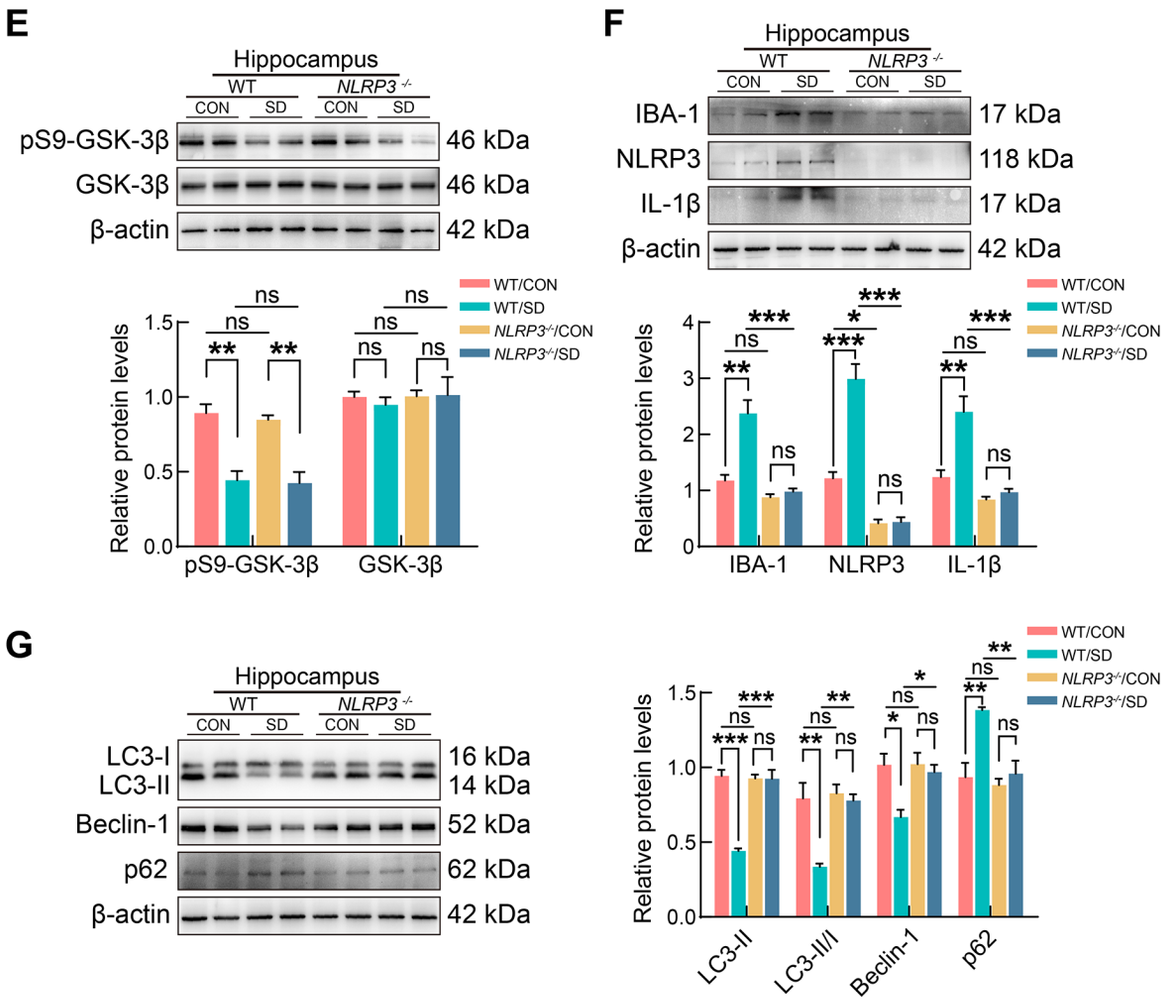

Figure 6 Behavioral and pathological changes induced by chronic SD were reversed in *NLRP3*$^{-/-}$ mice

A, B: Recognition index (A) and trajectory map (B) of WT/CON, WT/SD, *NLRP3*$^{-/-}$/CON, and *NLRP3*$^{-/-}$/SD mice in novel object recognition test. C: Protein levels of Tau-1, Tau-5, pS396-tau, and pT231-tau were determined by western blotting in hippocampus of WT/CON, WT/SD, *NLRP3*$^{-/-}$/CON, and *NLRP3*$^{-/-}$/SD mice. D: Representative immunofluorescence staining against pS396-tau was performed on hippocampal regions (CA1, CA3, and DG). Magnification ×10, Scale bar: 100 μm. E: Protein levels of p-GSK-3β (Ser9) and total GSK-3β were determined by western blotting in hippocampus. F: Protein levels of IBA-1, NLRP3, and IL-1β were determined by western blotting in hippocampus. G: Protein levels of Beclin-1, LC3-II, SQSTM1/p62, and LC3-II/LC3-I ratio were determined by western blotting in hippocampus. All data are expressed as mean±SEM. A, B: WT/CON n=8 mice/group; WT/SD n=6 mice/group; *NLRP3*$^{-/-}$/CON n=8 mice/group; *NLRP3*$^{-/-}$/SD n=7 mice/group. C–G: n=3 mice/group. β-actin was used as loading control in western blot analysis. Data were considered significant at *: P<0.05, **: P<0.01, ***: P<0.001, ****: P<0.0001. ns: Not significant. Means were compared using one-way ANOVA with Tukey's *post hoc* test. WT/CON: Normal sleep wild-type mice; WT/SD: Chronic sleep-deprived wild-type mice; *NLRP3*$^{-/-}$/CON: Normal sleep NLRP3 knockout mice; *NLRP3*$^{-/-}$/SD: Chronic sleep-deprived NLRP3 knockout mice.

Beclin-1, and SQSTM1/p62, or the ratio of LC3-II/LC3-I, were found in the hippocampus of *NLRP3*$^{-/-}$ mice following exposure to chronic SD (LC3-II: $F_{(3,8)}$=39.800, P<0.0001; WT/CON vs. WT/SD: P=0.0001; *NLRP3*$^{-/-}$/CON vs. *NLRP3*$^{-/-}$/SD: P>0.9999; WT/CON vs. *NLRP3*$^{-/-}$/CON: P=0.9887; WT/SD vs. *NLRP3*$^{-/-}$/SD: P=0.0001, LC3-II/I: $F_{(3,8)}$=13.451, P=0.0017; WT/CON vs. WT/SD: P=0.0041; *NLRP3*$^{-/-}$/CON vs. *NLRP3*$^{-/-}$/SD: P=0.9461; WT/CON vs. *NLRP3*$^{-/-}$/CON: P=0.9801; WT/SD vs. *NLRP3*$^{-/-}$/SD: P=0.0050, Beclin-1: $F_{(3,8)}$=5.130, P=0.0287; WT/CON vs. WT/SD: P=0.0192; *NLRP3*$^{-/-}$/CON vs. *NLRP3*$^{-/-}$/SD: P=0.9303; WT/CON vs. *NLRP3*$^{-/-}$/CON: P>0.9999; WT/SD vs. *NLRP3*$^{-/-}$/SD: P=0.0408, p62: $F_{(3,8)}$=11.600, P=0.0028; WT/CON vs. WT/SD: P=0.0069; *NLRP3*$^{-/-}$/CON vs. *NLRP3*$^{-/-}$/SD: P=0.8559; WT/CON vs. *NLRP3*$^{-/-}$/CON: P=0.9468; WT/SD vs. *NLRP3*$^{-/-}$/SD: P=0.0095, Figure 6G). Interestingly, the down-regulation of phosphorylated GSK-3β at the Ser9 site induced by chronic SD, which was observed in WT mice, reappeared in *NLRP3*$^{-/-}$ mice, suggesting that deletion of NLRP3 did not influence GSK-3β activation due to chronic SD (pS9-GSK-3β: $F_{(3,8)}$=19.091, P=0.0005; WT/CON vs. WT/SD: P=0.0026; *NLRP3*$^{-/-}$/CON vs. *NLRP3*$^{-/-}$/SD: P=0.0038; WT/CON vs. *NLRP3*$^{-/-}$/CON: P=0.9425; WT/SD vs. *NLRP3*$^{-/-}$/SD: P=0.9953, Figure 6E). In addition, chronic SD had no effect on the expression level of total GSK-3β in either WT or *NLRP3*$^{-/-}$ mice (t-GSK-3β: $F_{(3,8)}$=0.183, P=0.9051; WT/CON vs. WT/SD: P=0.9455; *NLRP3*$^{-/-}$/CON vs. *NLRP3*$^{-/-}$/SD: P=0.9999; WT/CON vs. *NLRP3*$^{-/-}$/CON: P>0.9999; WT/SD vs. *NLRP3*$^{-/-}$/SD: P=0.9093, Figure 6E).

Knockdown of NLRP3 in the hippocampus restored autophagic flux, suppressed tau hyperphosphorylation, and ameliorated cognitive deficits in chronic SD mice

To investigate the role of the NLRP3 inflammasome in the

brains of chronic SD mice, AAV-NLRP3 was stereotaxically microinjected into the hippocampus to achieve regional knockdown of NLRP3 expression.

Chronic SD mice injected with AAV-NLRP3 exhibited lower levels of IL-1β, NLRP3, and IBA-1 expression in the hippocampus than the chronic SD mice injected with AAV-GFP (IBA-1: t_4=7.323, P=0.0018; NLRP3: t_4=5.793, P=0.0044; IL-1β: t_4=8.199, P=0.0012, Figure 7A). Notably, a marked increase in the levels of Beclin-1, LC3-II, and the LC3-II/LC3-I ratio and a marked decrease in the level of SQSTM1/p62 were observed in the hippocampus of chronic SD mice injected with AAV-NLRP3 (Beclin-1: t_4=6.778, P=0.0025; LC3-II: t_4=5.719, P=0.0046; LC3-II/I: t_4=3.265, P=0.0309; p62: t_4=3.159, P=0.0342, Figure 7C). However, no differences were observed in the levels of phosphorylated GSK-3β at the Ser9 site and total GSK-3β between the chronic SD mice injected with AAV-NLRP3 and AAV-GFP, suggesting that hippocampal knockdown of NLRP3 had no influence on GSK-3β activity in chronic SD (pS9-GSK-3β: t_4=0.663, P=0.5436; t-GSK-3β: t_4=0.3517, P=0.7428, Figure 7B). Interestingly, AAV-NLRP3 microinjection significantly inhibited the chronic SD-induced increase in the expression of pT231-tau, pS396-tau, and Tau-5 and decrease in the expression of Tau-1 in the hippocampus of mice (pT231: t_4=4.336, P=0.0123; pS396: t_4=6.042, P=0.0038; Tau-1: t_4=8.420, P=0.0011; Tau-5: t_4=6.846, P=0.0024, Figure 7D, E). In addition, chronic SD mice injected with AAV-NLRP3 performed better in the discrimination test between familiar and novel objects compared to the chronic SD mice injected with AAV-GFP, as reflected by the significant increase in RI (t_{18}=3.426, P=0.0030, Cohen's d=1.532, Figure 7F, G).

Deletion of NLRP3 reversed NLRP3 inflammasome activation, autophagy deficits, and tau hyperphosphorylation caused by Akt inhibitor-induced activation of GSK-3β in primary hippocampal neurons

To determine the suitable dose and duration of the Akt inhibitor MK-2206, primary hippocampal neurons were treated with MK-2206 (250 nmol/L, 500 nmol/L, and 750 nmol/L) or 0.1% dimethyl sulfoxide (DMSO) and collected after 12, 24, and 48 h. Following MK-2206 treatment, a dose-dependent decrease was observed in the phosphorylation of the Akt downstream target GSK-3β (Ser9) at multiple time points (Figure 8A). A MK-2206 concentration of 250 nmol/L for 48 h was applied to treat primary hippocampal neurons derived from *NLRP3*$^{-/-}$ and WT mice in the following experiments.

The Akt inhibitor MK-2206 contributed to the pronounced activation of GSK-3β in primary hippocampal neurons, whether derived from *NLRP3*$^{-/-}$ or WT mice, as confirmed by the reduction in GSK-3β (Ser9) phosphorylation (pS9-GSK-3β: $F_{(3,8)}$=31.740, P<0.0001; t-GSK-3β: $F_{(3,8)}$=0.436, P=0.7335, Figure 8B). We next investigated the impact of MK-2206 treatment on the NLRP3 inflammasome. Of note, western blot analysis indicated that the NLRP3 and IL-1β protein expression levels were increased in the primary hippocampal neurons derived from WT mice after MK-2206 treatment, but were absent in the primary hippocampal neurons derived from *NLRP3*$^{-/-}$ mice, whether treated with vehicle or MK-2206 (NLRP3: $F_{(3,8)}$=46.752, P<0.0001; IL-1β: $F_{(3,8)}$=31.813, P=0.0004, Figure 8C). MK-2206 administration down-regulated the Beclin-1 and LC3-II protein expression levels, as well as the LC3-II/LC3-I ratio, and up-regulated the SQSTM1/p62 expression level in the primary hippocampal neurons derived from WT mice, with these effects inhibited in the primary hippocampal neurons derived from *NLRP3*$^{-/-}$ mice (LC3-II: $F_{(3,8)}$=19.462, P=0.0005; LC3-II/I: $F_{(3,8)}$=15.534, P=0.0011; Beclin-1: $F_{(3,8)}$=9.586, P=0.0050; p62: $F_{(3,8)}$=7.727, P=0.0095, Figure 8D). In addition, increased pT231-tau, pS396-tau, and Tau-5 expression and decreased Tau-1 expression were observed in the primary hippocampal neurons derived from WT mice after MK-2206 treatment, but were not found in the primary hippocampal neurons derived from *NLRP3*$^{-/-}$ mice (Tau-1: $F_{(3,8)}$=8.774, P=0.0065; Tau-5: $F_{(3,8)}$=8.656, P=0.0068; pT231: $F_{(3,8)}$=7.225, P=0.0115; pS396: $F_{(3,8)}$=6.263, P=0.0171, Figure 8E, F).

In summary, these results indicate that GSK-3β activation, induced by an Akt inhibitor, contributed to NLRP3 inflammasome activation, autophagy inhibition, and tau hyperphosphorylation in the primary hippocampal neurons derived from WT mice. However, those phenomena were reversed in the primary hippocampal neurons derived from *NLRP3*$^{-/-}$ mice.

DISCUSSION

Sleep is essential for maintaining homeostasis of the central nervous system. During sleep, the brain clears metabolic waste, processes information, and consolidates memories, allowing for optimal cognitive function (Fultz et al., 2019). Conversely, SD has been shown to impair cognitive function and heighten the risk of neurological disorders, such as AD. At present, however, the potential mechanisms linking SD to cognitive impairment remain poorly understood. In this study, we found that the gut microbiota composition in chronic SD mice differed markedly from that in WT controls. Specifically, gut microbiota derived from chronic SD mice exhibited significant alterations in the phyla Firmicutes, Bacteroidetes, and Proteobacteria, as well as in the genera *Lactobacillus* and *Odoribacter*. The Firmicutes-to-Bacteroidetes ratio, a key indicator of gut microbiota dysbiosis (Yang et al., 2015), was significantly reduced in chronic SD mice, similar to findings in the gut microbiota of AD mice and patients (Harach et al., 2017; Vogt et al., 2017), suggesting that an increased relative abundance of Bacteroidetes and a decreased relative abundance of Firmicutes may link chronic SD with AD. In addition, tau hyperphosphorylation and cognitive impairment were also observed in chronic SD mice. Interestingly, transferring gut microbiota derived from chronic SD mice led to tau aggregation and hyperphosphorylation and cognitive impairment in recipient mice. These findings indicate that the detrimental effects of chronic SD can be transmitted via gut microbiota, suggesting that changes in gut microbiota composition are secondary to chronic SD and play a direct pathogenetic role in tau hyperphosphorylation and cognitive impairment.

Tau is a microtubule-associated protein that promotes microtubule assembly and stability (Weingarten et al., 1975). Evidence indicates that overexpression of phosphorylated tau can damage neuronal synaptic plasticity and cause memory deficits (Li et al., 2019; Yin et al., 2016). In this study, phosphorylated tau at multiple sites, including Thr231 and Ser396, was markedly up-regulated and non-phosphorylated tau (Tau-1) was significantly down-regulated in the hippocampus of chronic SD mice. The aberrant aggregation of hyperphosphorylated tau can be attributed to two main factors: overexpression of tau kinases, especially GSK-3β, and disruption of tau clearance. Various studies on tau

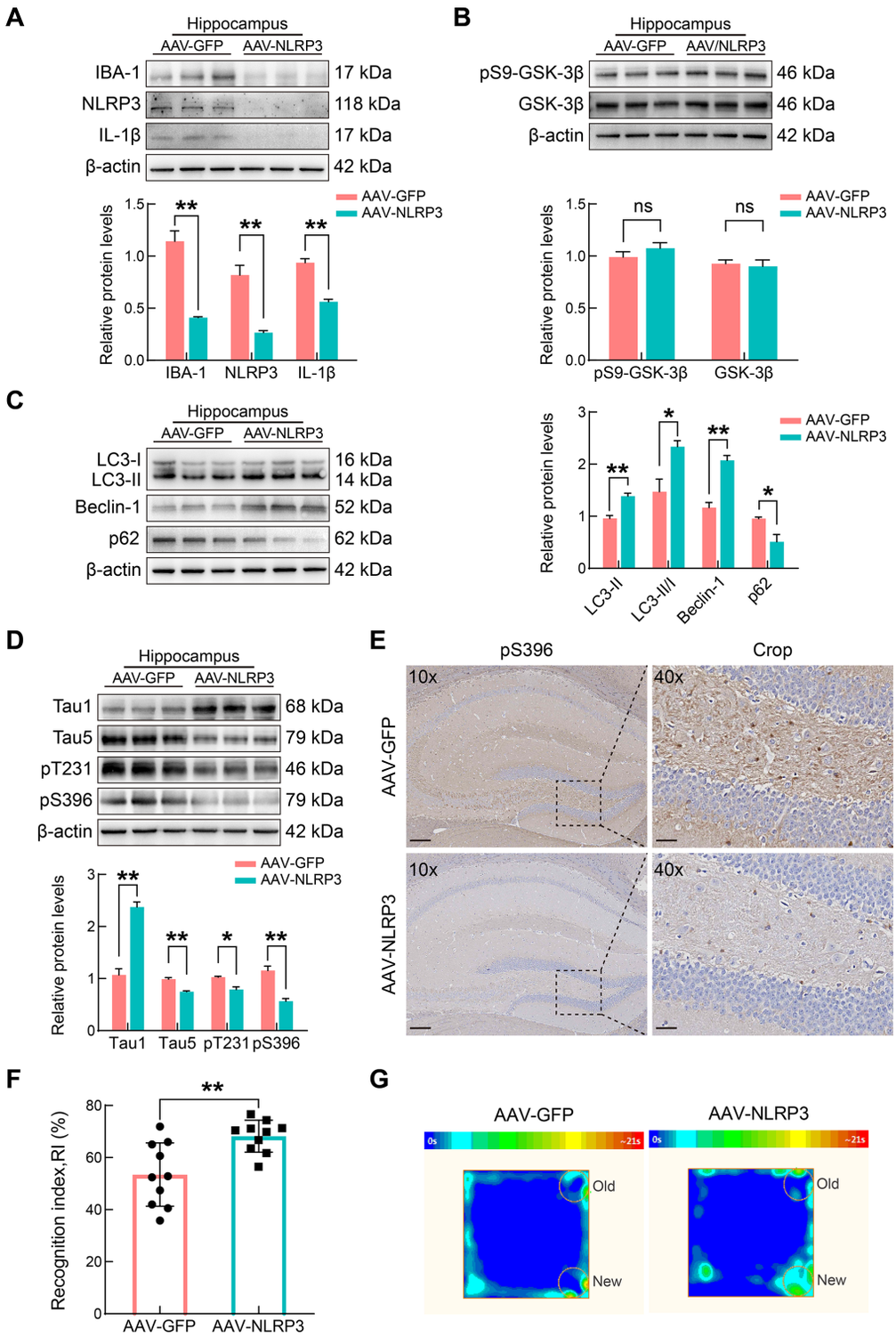

Figure 7 Knockdown of NLRP3 in the hippocampus restored autophagic flux, suppressed tau hyperphosphorylation, and ameliorated cognitive deficits

A: Protein levels of IBA-1, NLRP3, and IL-1β were determined by western blotting in hippocampus of chronic SD mice injected with AAV-GFP and chronic SD mice injected with AAV-NLRP3. B: Protein levels of p-GSK-3β (Ser9) and total GSK-3β were determined by western blotting in hippocampus of AAV-GFP and AAV-NLRP3 mice. C: Protein levels of Beclin-1, LC3-II, SQSTM1/p62, and LC3-II/LC3-I ratio were determined by western blotting in hippocampus of AAV-GFP and AAV-NLRP3 mice. D: Protein levels of Tau-1, Tau-5, pS396-tau, and pT231-tau were determined by western blotting in hippocampus of AAV-GFP and AAV-NLRP3 mice. E: Representative immunohistochemical staining against pS396-tau were performed on hippocampal regions (CA1, CA3, and DG). Magnification ×10, Scale bar: 100 μm. Magnification ×40, Scale bar: 25 μm. F, G: Recognition index (F) and trajectory map (G) of AAV-GFP and AAV-NLRP3 mice in novel object recognition test. All data are expressed as mean±SEM. A–E: n=3 mice/group. F, G: n=10 mice/group. β-actin was used as loading control in western blot analysis. Data are considered significant at *: P<0.05, **: P<0.01, ***: P<0.001, ****: P<0.0001. ns: Not significant. Means were compared using Student's t-test. AAV-GFP: Chronic sleep-deprived mice injected with AAV-GFP; AAV-NLRP3: Chronic sleep-deprived mice injected with AAV-NLRP3.

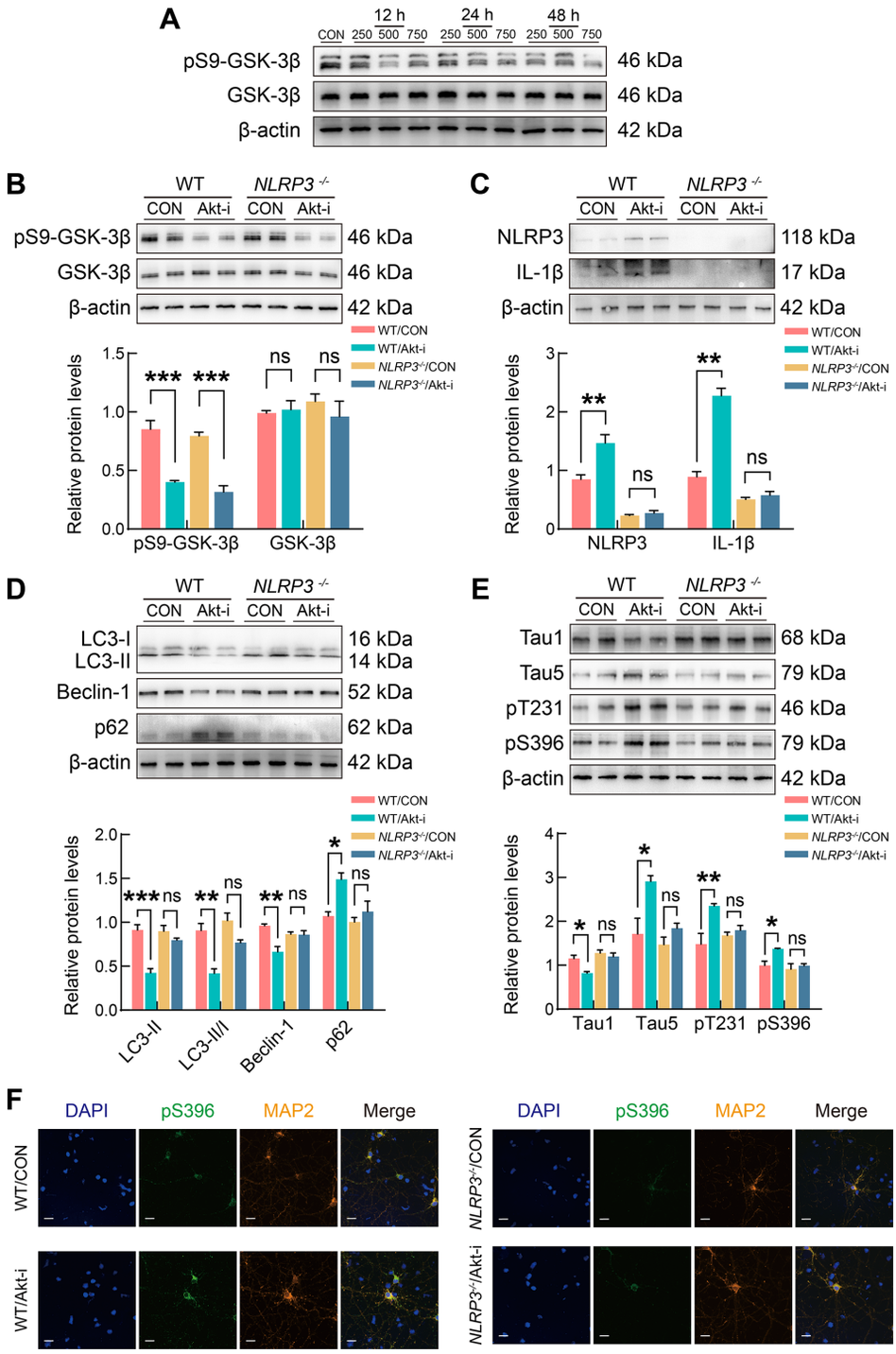

Figure 8 Deletion of NLRP3 reversed NLRP3 inflammasome activation, autophagy deficits, and tau hyperphosphorylation caused by Akt inhibitor-induced activation of GSK-3β in primary hippocampal neurons

A: Primary hippocampal neurons were treated with Akt inhibitor MK-2206 (250 nmol/L, 500 nmol/L, and 750 nmol/L) or 0.1% dimethyl sulfoxide (DMSO) and collected after 12, 24, and 48 h. Western blotting was conducted to assess expression levels of p-GSK-3β (Ser9) and total GSK-3β. B: Protein levels of p-GSK-3β (Ser9) and total GSK-3β were determined by western blotting in primary hippocampal neurons obtained from WT and *NLRP3*$^{-/-}$ mice with or without Akt inhibitor treatment. C: Protein levels of IBA-1, NLRP3, and IL-1β were determined by western blotting in four groups. D: Protein levels of Beclin-1, LC3-II, SQSTM1/p62, and LC3-II/LC3-I ratio were determined by western blotting in four groups. E: Protein levels of Tau-1, Tau-5, pS396-tau, and pT231-tau were determined by western blotting in four groups. F: Representative immunofluorescence staining against pS396-tau was performed on primary hippocampal neurons. Magnification ×60, Scale bar: 20 μm. All data are expressed as mean±SEM. *n*=3 independent experiments for each group. β-actin was used as loading control in western blot analysis. Data are considered significant at *: *P*<0.05, **: *P*<0.01, ***: *P*<0.001, ****: *P*<0.0001. ns: Not significant. Means were compared using one-way ANOVA with Tukey's *post hoc* test. WT/CON: Primary hippocampal neurons obtained from WT mice without Akt inhibitor treatment; WT/Akt-i: Primary hippocampal neurons obtained from WT mice with Akt inhibitor treatment; *NLRP3*$^{-/-}$/CON: Primary hippocampal neurons obtained from *NLRP3*$^{-/-}$ mice without Akt inhibitor treatment; *NLRP3*$^{-/-}$/Akt-i: Primary hippocampal neurons obtained from *NLRP3*$^{-/-}$ mice with Akt inhibitor treatment.

hyperphosphorylation have identified GSK-3β as a key kinase in tau hyperphosphorylation, as GSK-3β-mediated tau phosphorylation promotes toxic self-aggregation (L'episcopo et al., 2016; Martin et al., 2013). The autophagy-lysosome system is also a crucial mechanism for tau clearance. Both *in vitro* and *in vivo* findings have shown that inhibition of autophagic flux impedes tau clearance, leading to the aggregation of insoluble tau proteins (Hamano et al., 2021). Interestingly, chronic SD increased the level of total tau without affecting its mRNA level, suggesting that chronic SD disturbs tau clearance. We found that chronic SD inhibited autophagic flux and activated GSK-3β in the brain. Similarly, colonization with "SD microbiota" led to autophagy dysfunction and GSK-3β activation in the hippocampus of recipient mice. These findings suggest that GSK-3β activation and autophagy dysfunction are involved in gut microbiota dysbiosis-mediated tau pathology in chronic SD.

The gut microbiota produces a significant amount of harmful microbial products and metabolites, which trigger peripheral and central inflammatory responses (Blander et al., 2017). The NLRP3 inflammasome is considered an important signaling interface that mediates inflammation upon recognition of microbial or danger-associated molecular stimuli (Liao et al., 2019; Sendler et al., 2020). Activation of the NLRP3 inflammasome leads to the autocleavage and activation of caspase-1, which induces the maturation and release of IL-1β (Paik et al., 2021). IL-1β, a proinflammatory cytokine, is regulated by NLRP3 inflammasome activation, and its production is markedly inhibited in *NLRP3*$^{-/-}$ mice (Fujimura et al., 2023). When NLRP3/IL-1β signaling is inappropriately activated or overactivated, it creates a chronic inflammatory environment that drives the pathogenesis and progression of many diseases, including age-related diseases, Parkinson's disease, and AD. Overactivation of the NLRP3 inflammasome and subsequent secretion of IL-1β in microglia mediates neuroinflammation, which drives the hyperphosphorylation and aggregation of tau, accelerating AD progression (Ising et al., 2019). Thus, we hypothesize that the NLRP3 inflammasome is a crucial node linking gut microbiota dysbiosis to tau pathology and cognitive deficits in chronic SD. In this study, we found that chronic SD enhanced NLRP3 inflammasome activity. Similarly, colonization with "SD microbiota" led to the overexpression of the NLRP3 inflammasome. To investigate whether the NLRP3 inflammasome is a crucial node linking gut microbiota dysbiosis to tau pathology and cognitive impairment in chronic SD, we used *NLRP3*$^{-/-}$ mice. Results showed that, following chronic SD, cognitive function was significantly impaired in WT mice but not in *NLRP3*$^{-/-}$ mice. Additionally, autophagy dysfunction and tau hyperphosphorylation observed in WT mice following chronic SD were reversed in *NLRP3*$^{-/-}$ mice. Consistently, specific knockdown of NLRP3 in the hippocampus restored autophagic flux, suppressed tau hyperphosphorylation, and ameliorated cognitive deficits in chronic SD mice. These findings demonstrate that the NLRP3 inflammasome is a core regulator of autophagy, which, in turn, regulates the aggregation and phosphorylation of tau in cognitive deficits resulting from chronic SD. Taken together, these results indicate that alterations in gut microbiota exposed to chronic SD can lead to tau aggregation and hyperphosphorylation primarily by triggering NLRP3-mediated autophagy dysfunction, ultimately causing cognitive impairment.

Interestingly, the deletion of NLRP3 in *NLRP3*$^{-/-}$ mice and the regional knockdown of NLRP3 in the hippocampus had no effect on GSK-3β activation due to chronic SD, suggesting that GSK-3β activity is not regulated by the NLRP3 inflammasome under chronic SD conditions. Recent evidence has highlighted the role of GSK-3β as a regulator of adaptive and innate immune responses (Beurel et al., 2010). GSK-3β modulates the Toll-like receptor-mediated inflammatory response and differentially regulates the production of pro-inflammatory and anti-inflammatory cytokines (Martin et al., 2005; Rehani et al., 2009). Furthermore, GSK-3β activation promotes the migration and activation of microglia and astrocytes, with its up-regulation in these cells increasing several proinflammatory cytokines, including IL-1, IL-6, and tumor necrosis factor α (TNF-α) (Beurel & Jope, 2009; Renault-Mihara et al., 2011; Wang et al., 2010). In addition, accumulating evidence indicates that GSK-3β may be involved in NLRP3 inflammasome activation in various diseases, including lupus nephritis, myocardial infarction, and cerebral ischemia/reperfusion injury (Arumugam et al., 2022; Wang et al., 2020, 2022). This suggests that GSK-3β may be the upstream regulator of the NLRP3 inflammasome, triggering its activation in chronic SD. To explore the potential connections between GSK-3β and the NLRP3 inflammasome, we treated primary hippocampal neurons derived from WT and *NLRP3*$^{-/-}$ mice with the Akt inhibitor MK-2206. The serine/threonine kinase Akt, also known as protein kinase B (PKB), is a central node in many signaling pathways and modulates the function of many downstream proteins (Tsai et al., 2022). GSK-3β is a critical downstream target of Akt. When Akt is activated, it phosphorylates GSK-3β at the Ser9 site, resulting in GSK-3β inhibition (Manning & Toker, 2017). Given the lack of a direct GSK-3β agonist, we used the Akt inhibitor MK-2206 to achieve GSK-3β activation. As expected, MK-2206 administration down-regulated the phosphorylation of GSK-3β (Ser9), resulting in its activation. GSK-3β activation via Akt inhibition contributed to NLRP3 inflammasome activation, autophagy inhibition, and tau hyperphosphorylation in primary hippocampal neurons derived from WT mice. However, those effects were reversed in primary hippocampal neurons derived from *NLRP3*$^{-/-}$ mice. These findings indicate that GSK-3β is not only a tau kinase but also a regulator of the NLRP3 inflammasome, triggering its activation under chronic SD conditions. GSK-3β also acts as a tau kinase and regulator of NLRP3-mediated autophagy dysfunction, co-promoting tau hyperphosphorylation. Although GSK-3β remained activated, the improved autophagy induced by NLRP3 deficiency was sufficient to suppress tau hyperphosphorylation. Thus, GSK-3β plays a significant role in promoting tau hyperphosphorylation and aggregation by regulating NLRP3-mediated autophagy dysfunction.

In summary, chronic SD leads to gut microbiota dysbiosis, which subsequently triggers GSK-3β activation in the brain. Activated GSK-3β functions as both a tau kinase and a regulator of NLRP3-mediated autophagy dysfunction, promoting tau hyperphosphorylation and aggregation, ultimately resulting in cognitive impairment. To the best of our knowledge, this study is the first to identify gut microbiota dysbiosis as a key driver of tau pathology via NLRP3-mediated autophagy dysfunction in chronic SD, contributing to cognitive deficits. Future research should explore intervention strategies targeting gut microbiota composition, NLRP3 inflammasome activation, and tau pathology to mitigate the

detrimental consequences of chronic SD. Our study highlights the role of GSK-3β as a regulator of NLRP3-mediated autophagy dysfunction, which promotes tau hyperphosphorylation and aggregation.

This study also has some limitations. First, we only investigated the effects of chronic SD on gut microbiota using animal models. However, it would be beneficial to include human subjects for clinical validation. Additionally, while our research focused on the molecular mechanisms in the brain regulated by gut microbiota dysbiosis in chronic SD, we did not examine the peripheral pathways through which gut microbiota affects the brain, which warrants further investigation.

SUPPLEMENTARY DATA

Supplementary data to this article can be found online.

COMPETING INTERESTS

The authors declare that they have no competing interests.

AUTHORS' CONTRIBUTIONS

N.Z. designed the research, conducted the experiments, acquired and analyzed the data, and wrote the manuscript. X.C. conducted the experiments and acquired and analyzed the data. Q.G.C. conducted the experiments. X.T.L. and F.G. analyzed the data. M.M.Z. acquired the reagents. F.L.Y. and Z.J.Z. reviewed the manuscript. Q.G.R designed the research and reviewed the manuscript. All authors read and approved the final version of the manuscript.

ACKNOWLEDGMENTS

We thank Hai-Long Zhao for technical support.

REFERENCES

Agirman G, Yu KB, Hsiao EY. 2021. Signaling inflammation across the gut-brain axis. *Science*, **374**(6571): 1087–1092.

Arumugam S, Qin YQ, Liang ZW, et al. 2022. GSK3β mediates the spatiotemporal dynamics of NLRP3 inflammasome activation. *Cell Death & Differentiation*, **29**(10): 2060–2069.

Avila J, Lucas JJ, Pérez M, et al. 2004. Role of tau protein in both physiological and pathological conditions. *Physiological Reviews*, **84**(2): 361–384.

Barthélemy NR, Liu HY, Lu W, et al. 2020. Sleep deprivation affects tau phosphorylation in human cerebrospinal fluid. *Annals of Neurology*, **87**(5): 700–709.

Benedict C, Vogel H, Jonas W, et al. 2016. Gut microbiota and glucometabolic alterations in response to recurrent partial sleep deprivation in normal-weight young individuals. *Molecular Metabolism*, **5**(12): 1175–1186.

Beurel E, Jope RS. 2009. Lipopolysaccharide-induced interleukin-6 production is controlled by glycogen synthase kinase-3 and STAT3 in the brain. *Journal of Neuroinflammation*, **6**: 9.

Beurel E, Michalek SM, Jope RS. 2010. Innate and adaptive immune responses regulated by glycogen synthase kinase-3 (GSK3). *Trends in Immunology*, **31**(1): 24–31.

Biasizzo M, Kopitar-Jerala N. 2020. Interplay between NLRP3 inflammasome and autophagy. *Frontiers in Immunology*, **11**: 591803.

Blander JM, Longman RS, Iliev ID, et al. 2017. Regulation of inflammation by microbiota interactions with the host. *Nature Immunology*, **18**(8): 851–860.

Bowers SJ, Vargas F, González A, et al. 2020. Repeated sleep disruption in mice leads to persistent shifts in the fecal microbiome and metabolome. *PLoS One*, **15**(2): e0229001.

Cosin-Roger J, Simmen S, Melhem H, et al. 2017. Hypoxia ameliorates intestinal inflammation through NLRP3/mTOR downregulation and autophagy activation. *Nature Communications*, **8**(1): 98.

Cryan JF, O'riordan KJ, Cowan CSM, et al. 2019. The microbiota-gut-brain axis. *Physiological Reviews*, **99**(4): 1877–2013.

Donlea JM. 2019. Roles for sleep in memory: insights from the fly. *Current Opinion in Neurobiology*, **54**: 120–126.

El Aidy S, Bolsius YG, Raven F, et al. 2020. A brief period of sleep deprivation leads to subtle changes in mouse gut microbiota. *Journal of Sleep Research*, **29**(6): e12920.

Feng YS, Tan ZX, Wu LY, et al. 2020. The involvement of NLRP3 inflammasome in the treatment of Alzheimer's disease. *Ageing Research Reviews*, **64**: 101192.

Fujimura K, Karasawa T, Komada T, et al. 2023. NLRP3 inflammasome-driven IL-1β and IL-18 contribute to lipopolysaccharide-induced septic cardiomyopathy. *Journal of Molecular and Cellular Cardiology*, **180**: 58–68.

Fultz NE, Bonmassar G, Setsompop K, et al. 2019. Coupled electrophysiological, hemodynamic, and cerebrospinal fluid oscillations in human sleep. *Science*, **366**(6465): 628–631.

Hamano T, Enomoto S, Shirafuji N, et al. 2021. Autophagy and Tau protein. *International Journal of Molecular Sciences*, **22**(14): 7475.

Hamano T, Gendron TF, Causevic E, et al. 2008. Autophagic-lysosomal perturbation enhances tau aggregation in transfectants with induced wild-type tau expression. *European Journal of Neuroscience*, **27**(5): 1119–1130.

Harach T, Marungruang N, Duthilleul N, et al. 2017. Reduction of Abeta amyloid pathology in APPPS1 transgenic mice in the absence of gut microbiota. *Scientific Reports*, **7**: 41802.

Holth JK, Fritschi SK, Wang C, et al. 2019. The sleep-wake cycle regulates brain interstitial fluid tau in mice and CSF tau in humans. *Science*, **363**(6429): 880–884.

Ising C, Venegas C, Zhang SS, et al. 2019. NLRP3 inflammasome activation drives tau pathology. *Nature*, **575**(7784): 669–673.

Kaushik S, Cuervo AM. 2015. Proteostasis and aging. *Nature Medicine*, **21**(12): 1406–1415.

Kim MS, Kim Y, Choi H, et al. 2020. Transfer of a healthy microbiota reduces amyloid and tau pathology in an Alzheimer's disease animal model. *Gut*, **69**(2): 283–294.

Krueger JM, Frank MG, Wisor JP, et al. 2016. Sleep function: toward elucidating an enigma. *Sleep Medicine Reviews*, **28**: 46–54.

Lachance V, Wang Q, Sweet E, et al. 2019. Autophagy protein NRBF2 has reduced expression in Alzheimer's brains and modulates memory and amyloid-beta homeostasis in mice. *Molecular Neurodegeneration*, **14**(1): 43.

L'episcopo F, Drouin-Ouellet J, Tirolo C, et al. 2016. GSK-3*β*-induced Tau pathology drives hippocampal neuronal cell death in Huntington's disease: involvement of astrocyte-neuron interactions. *Cell Death & Disease*, **7**: e2206.

Levine B, Kroemer G. 2019. Biological functions of autophagy genes: a disease perspective. *Cell*, **176**(1-2): 11–42.

Li XG, Hong XY, Wang YL, et al. 2019. Tau accumulation triggers STAT1-dependent memory deficits by suppressing NMDA receptor expression. *EMBO Reports*, **20**(6): e47202.

Liao LJ, Schneider KM, Galvez EJC, et al. 2019. Intestinal dysbiosis augments liver disease progression via NLRP3 in a murine model of primary sclerosing cholangitis. *Gut*, **68**(8): 1477–1492.

Liu Z, Wei ZY, Chen JY, et al. 2020. Acute sleep-wake cycle shift results in community alteration of human gut microbiome. *mSphere*, **5**(1): e00914–19.

Lo JC, Ong JL, Leong RLF, et al. 2016. Cognitive performance, sleepiness, and mood in partially sleep deprived adolescents: the need for sleep study. *Sleep*, **39**(3): 687–698.

Lucey BP, Wisch J, Boerwinkle AH, et al. 2021. Sleep and longitudinal cognitive performance in preclinical and early symptomatic Alzheimer's disease. *Brain*, **144**(9): 2852–2862.

Manning BD, Toker A. 2017. AKT/PKB signaling: navigating the network. *Cell*, **169**(3): 381–405.

Martin L, Latypova X, Wilson CM, et al. 2013. Tau protein kinases: involvement in Alzheimer's disease. *Ageing Research Reviews*, **12**(1): 289–309.

Martin M, Rehani K, Jope RS, et al. 2005. Toll-like receptor-mediated cytokine production is differentially regulated by glycogen synthase kinase 3. *Nature Immunology*, **6**(8): 777–784.

Mayer EA, Nance K, Chen S. 2022. The gut-brain axis. *Annual Review of Medicine*, **73**: 439–453.

Morais LH, Schreiber HL, Mazmanian SK. 2021. The gut microbiota-brain axis in behaviour and brain disorders. *Nature Reviews Microbiology*, **19**(4): 241–255.

Paik S, Kim JK, Silwal P, et al. 2021. An update on the regulatory mechanisms of NLRP3 inflammasome activation. *Cellular & Molecular Immunology*, **18**(5): 1141–1160.

Pearson-Leary J, Zhao CY, Bittinger K, et al. 2020. The gut microbiome regulates the increases in depressive-type behaviors and in inflammatory processes in the ventral hippocampus of stress vulnerable rats. *Molecular Psychiatry*, **25**(5): 1068–1079.

Pellegrini C, Antonioli L, Calderone V, et al. 2020. Microbiota-gut-brain axis in health and disease: is NLRP3 inflammasome at the crossroads of microbiota-gut-brain communications?. *Progress in Neurobiology*, **191**: 101806.

Pellegrini C, Antonioli L, Colucci R, et al. 2018. Interplay among gut microbiota, intestinal mucosal barrier and enteric neuro-immune system: a common path to neurodegenerative diseases?. *Acta Neuropathologica*, **136**(3): 345–361.

Polito VA, Li HM, Martini-Stoica H, et al. 2014. Selective clearance of aberrant tau proteins and rescue of neurotoxicity by transcription factor EB. *EMBO Molecular Medicine*, **6**(9): 1142–1160.

Poroyko VA, Carreras A, Khalyfa A, et al. 2016. Chronic sleep disruption alters gut microbiota, induces systemic and adipose tissue inflammation and insulin resistance in mice. *Scientific Reports*, **6**: 35405.

Rehani K, Wang HZ, Garcia CA, et al. 2009. Toll-like receptor-mediated production of IL-1Ra is negatively regulated by GSK_3 via the MAPK ERK1/2. *The Journal of Immunology*, **182**(1): 547–553.

Renault-Mihara F, Katoh H, Ikegami T, et al. 2011. Beneficial compaction of spinal cord lesion by migrating astrocytes through glycogen synthase kinase-3 inhibition. *EMBO Molecular Medicine*, **3**(11): 682–696.

Robbins R, Quan SF, Weaver MD, et al. 2021. Examining sleep deficiency and disturbance and their risk for incident dementia and all-cause mortality in older adults across 5 years in the United States. *Aging*, **13**(3): 3254–3268.

Scheltens P, De Strooper B, Kivipelto M, et al. 2021. Alzheimer's disease. *The Lancet*, **397**(10284): 1577–1590.

Sendler M, Van Den Brandt C, Glaubitz J, et al. 2020. NLRP3 inflammasome regulates development of systemic inflammatory response and compensatory anti-inflammatory response syndromes in mice with acute pancreatitis. *Gastroenterology*, **158**(1): 253–269. e14.

Shi L, Chen SJ, Ma MY, et al. 2018. Sleep disturbances increase the risk of dementia: a systematic review and meta-analysis. *Sleep Medicine Reviews*, **40**: 4–16.

Spillantini MG, Goedert M. 2013. Tau pathology and neurodegeneration. *The Lancet Neurology*, **12**(6): 609–622.

Tang MM, Liu T, Jiang P, et al. 2021. The interaction between autophagy and neuroinflammation in major depressive disorder: from pathophysiology to therapeutic implications. *Pharmacological Research*, **168**: 105586.

Tsai PJ, Lai YH, Manne RK, et al. 2022. Akt: a key transducer in cancer. *Journal of Biomedical Science*, **29**(1): 76.

Vogt NM, Kerby RL, Dill-Mcfarland KA, et al. 2017. Gut microbiome alterations in Alzheimer's disease. *Scientific Reports*, **7**(1): 13537.

Vuotto C, Battistini L, Caltagirone C, et al. 2020. Gut microbiota and disorders of the central nervous system. *The Neuroscientist*, **26**(5-6): 487–502.

Wadhwa M, Prabhakar A, Anand JP, et al. 2019. Complement activation sustains neuroinflammation and deteriorates adult neurogenesis and spatial memory impairment in rat hippocampus following sleep deprivation. *Brain, Behavior, and Immunity*, **82**: 129–144.

Wang DY, Zhang JB, Jiang WK, et al. 2017. The role of NLRP3-CASP1 in inflammasome-mediated neuroinflammation and autophagy dysfunction in manganese-induced, hippocampal-dependent impairment of learning and memory ability. *Autophagy*, **13**(5): 914–927.

Wang MJ, Huang HY, Chen WF, et al. 2010. Glycogen synthase kinase-3β inactivation inhibits tumor necrosis factor-α production in microglia by modulating nuclear factor κB and MLK3/JNK signaling cascades. *Journal of Neuroinflammation*, **7**: 99.

Wang SH, Cui LG, Su XL, et al. 2022. GSK-3β-mediated activation of NLRP3 inflammasome leads to pyroptosis and apoptosis of rat cardiomyocytes and fibroblasts. *European Journal of Pharmacology*, **920**: 174830.

Wang SH, Su XL, Xu LN, et al. 2020. Glycogen synthase kinase-3β inhibition alleviates activation of the NLRP3 inflammasome in myocardial infarction. *Journal of Molecular and Cellular Cardiology*, **149**: 82–94.

Wang Z, Chen WH, Li SX, et al. 2021. Gut microbiota modulates the inflammatory response and cognitive impairment induced by sleep deprivation. *Molecular Psychiatry*, **26**(11): 6277–6292.

Weingarten MD, Lockwood AH, Hwo SY, et al. 1975. A protein factor essential for microtubule assembly. *Proceedings of the National Academy of Sciences of the United States of America*, **72**(5): 1858–1862.

Wu AG, Zhou XG, Qiao G, et al. 2021. Targeting microglial autophagic degradation in NLRP3 inflammasome-mediated neurodegenerative diseases. *Ageing Research Reviews*, **65**: 101202.

Yang T, Santisteban MM, Rodriguez V, et al. 2015. Gut dysbiosis is linked to hypertension. *Hypertension*, **65**(6): 1331–1340.

Yin MM, Chen YL, Zheng H, et al. 2017. Assessment of mouse cognitive and anxiety-like behaviors and hippocampal inflammation following a repeated and intermittent paradoxical sleep deprivation procedure. *Behavioural Brain Research*, **321**: 69–78.

Yin YL, Gao D, Wang YL, et al. 2016. Tau accumulation induces synaptic impairment and memory deficit by calcineurin-mediated inactivation of nuclear CaMKIV/CREB signaling. *Proceedings of the National Academy of Sciences of the United States of America*, **113**(26): E3773–E3781.

Zhang L, Wang Y, Xia XY, et al. 2017. Altered gut microbiota in a mouse model of Alzheimer's disease. *Journal of Alzheimers Disease*, **60**(4): 1241–1257.

Zhang Y, Huang RR, Cheng MJ, et al. 2019. Gut microbiota from NLRP3-deficient mice ameliorates depressive-like behaviors by regulating astrocyte dysfunction via circHIPK2. *Microbiome*, **7**(1): 116.

Zhang ZG, Yang XF, Song YQ, et al. 2021. Autophagy in Alzheimer's disease pathogenesis: therapeutic potential and future perspectives. *Ageing Research Reviews*, **72**: 101464.

Zhao N, Chen QG, Chen X, et al. 2023. Intestinal dysbiosis mediates cognitive impairment via the intestine and brain NLRP3 inflammasome activation in chronic sleep deprivation. *Brain, Behavior, and Immunity*, **108**: 98–117.

Zhuang ZQ, Shen LL, Li WW, et al. 2018. Gut microbiota is altered in patients with Alzheimer's disease. *Journal of Alzheimers Disease*, **63**(4): 1337–1346.